Multi-objective-based economic dispatch and loss reduction in the presence of electric vehicles considering different optimization techniques

David Hmingthanmawia[1], Subhasish Deb[1]*, Subir Datta[1], Ksh. Robert Singh[1], Umit Cali[2,3]* and Taha Selim Ustun[4]*

[1]Department of Electrical Engineering, Mizoram University, Aizawl, Mizoram, India, [2]Department of Electric Energy, Norwegian University of Science and Technology, Trondheim, Norway, [3]School of Physics, Engineering an Technology, University of York, York, United Kingdom, [4]Fukushima Renewable Energy Institute, AIST (FREA), Koriyama, Japan

Currently, electric vehicles (EVs) are the most liked mode for green transportation. However, the vehicle-to-grid (V2G) technology can reduce the peak demand on the power grid, which is an efficient way to encourage the integration of EVs. This paper proposes a multi-objective-based economic dispatch management including EVs to minimize the generator cost and active power loss. The entire system is retained for keeping in mind the economic operation of the whole system. Then, EVs are introduced to the system, taking into account vehicle requirements and load demands and considering EV constraints. The target of the proposed work is to demonstrate how effectively large-scale EVs can participate in valley filling and peak load shaving along with multi-objective-based cost and loss reduction. The proposed optimization problem is employed in an IEEE 30-bus system. The multi-objective grasshopper optimization algorithm and the ant-lion optimization are compared to observe the minimum cost and total loss of the system. The results show that the total generation cost and power loss of the system decrease due to the V2G mode of operation. In addition, EVs provide an alternative method for dealing with peak load, while filling the off-peak hours effectively. The total generation cost and power loss for 24 h using MOGOA without implementation of EVs are 8,757.128 $/hr and 65.28509 MW, respectively, and with EVs, the total generation cost and power loss for 24 h are 8,617.077 $/hr and 55.65349 MW, respectively. Thus, with the implementation of EVs, the total generation cost reduced by 1.59% and the total power loss reduced by 14.75%, and with MOALO, the total generation cost and power loss for 24 h without EVs are 8,977.077 $/hr and 44.20877 MW, respectively, and with EVs, the total generation cost and power loss for 24 h are 8,923.529 $/hr and 41.69524 MW, respectively. Thus, with the implementation of EVs, the total generation cost reduced by 0.59% and the total power loss reduced by 5.68%.

The analysis of the results demonstrates how effectively EVs in the V2G mode can reduce the dependency over the grid power during the time of peak load demand.

GRAPHICAL ABSTRACT
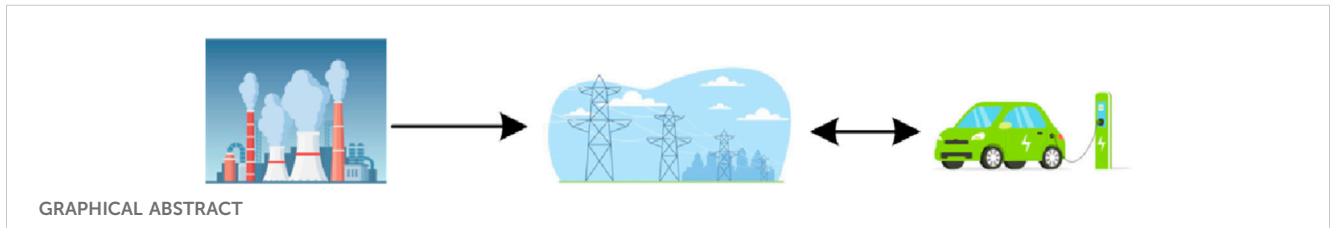
1 Introduction

The goal of economic dispatch (ED), which is a crucial task in power systems and is essentially a multi-objective optimization problem, is to determine the best schedule for generators to minimize the overall fuel cost under specific limitations, including loss in the system (Jayabarathi et al., 2016; Latif et al., 2020). Minimization of generation costs is the goal of the significant, practical optimization problem known as economic dispatch in power systems (Dey et al., 2020). Given the significance of ED, efforts to solve the ED problem date back to the early 1970s. ED can be resolved using the gradient method, the projection method, and the λ-iteration method as a restricted optimization problem (Wood et al., 2012). In the studies by Chiang (2005) and Sahoo et al. (2024), the existence of forbidden operation zones is one of the requirements that the ED problem must meet. Bahrani and Patra (2017) used the orthogonal PSO (OPSO) algorithm for solving the ED problem by taking three power systems under several power constraints imposed by thermal generating units (TGUs) and smart power grid (SPG), for example, ramp rate limits and prohibited operating zones. Chatuanramtharnghaka et al. (2021) used a multi-objective optimization method called grasshopper optimization algorithm (GOA) to manage congestion in the system transmission line. The algorithm adjusts parameters to ensure that the system operates at the lowest possible cost. Sahoo et al. (2023) investigated the role of flexible AC transmission systems in managing congestions in a deregulated market for different topologies. Latif et al. (2021) estimated the optimal power dispatch for a marine microgrid using the GOA. The findings when contrasted with those of the most popular and contemporary algorithms demonstrate that the GOA produces more robust results that capture more renewables and provides more stability. Lalhmachhuana et al. (2024) utilized a multi-objective engineering design issue to apply MOALO, which is contrasted with MOPSO. The findings demonstrate how the excellent convergence and coverage of the GOA help its test functions. The algorithm's performance on economic and emission dispatch problems shows how well it works to solve difficult real-world issues as well.

Sen and Mathur (2016) suggested a better method for creating artificial bee colonies (ABCs) to address the dynamic economic emission dispatch (DEED) issue. The suggested method provides superior optimum solutions when compared to over ten metaheuristic techniques, according to the results. The problem of environmental issues and the energy crisis has drawn significant attention to PEVs as a crucial component for future power systems (Safiullah et al., 2022; Xing et al., 2016). However, as PEV charging habits are variable, when more PEVs are sold, the peak–valley load disparity will widen even more, increasing the load demand (Ranjan et al., 2021; Ma et al., 2017). Tappeta et al. (2022) examined the framework of the V2G technology and its advantages, drawbacks, and optimization techniques. The authors concluded that V2G can assist the electricity system with peak load cutting and load leveling. Hussain et al. (2020) showed that with V2G, air pollution and power outages can be reduced, system efficiency can be increased, and the grid can become more stable and dependable. They play a critical role in supporting supply and demand balancing by reducing peaks and filling valleys. The EV batteries can be charged during the evenings, when there is less demand (Han et al., 2010a). The bidirectional inductive power transfer (IPT) charger is developed by Madawala and Thrimawithana (2011) with a control system that may be utilized to set a boundary for the maximum value of the primary side current when it increases, thereby safeguarding the IPT system. Srivastava et al. (2010) addressed the various modeling approaches and optimization techniques used in the studies of the market penetration rates of electric vehicles, hybrid electric vehicles, plug-in hybrid electric vehicles, and battery electric vehicles. Sioshansi and Denholm (2009) conducted an in-depth review of the current state of EVs and related grid-interfacing technologies in the literature. The primary conclusions and data information are taken from recent publications that emphasize the most recent developments in technology, their drawbacks, and possible directions for future market growth. Kempton and Tomic (2005) determined the grid power capacities of three different types of electric drive cars by the developed formulae. The revenue and expenses that supply electricity to different electric marketplaces are assessed using these equations. Han et al. (2010b) examined the response of EVs in frequency regulation. Certain distinct scenarios have been taken into account when assessing the impact of disturbances in system frequency: the non-availability of grid-connected EVs and EVs that provide frequency response. Nsonga et al. (2017) suggested a methodical strategy in which

every charging and discharging sequence for electric vehicles is recognized.

Following that, ratings and suggestions on which tactics to use for particular purposes are also given. The viability of charging PHEVs at off-peak hours on Ontario's grid is examined (Hajimiragha et al., 2010). By storing surplus energy generated during windy periods and delivering it back into the grid during times of high demand, V2G can be used to buffer renewable energy sources, such as wind turbine generators. This essentially stabilizes the alternating nature of wind power. Kempton et al. suggested using V2G for electric vehicles, in which it enabled the EVs to function as part of the power system (Kempton and Letendre, 1997; Ustun et al., 2021). When EVs take part in V2G, they can charge at a lower cost during off-peak hours and absorb more energy as an allocated battery to stabilize the power grid. When peak load demands arise, the discharge function is then utilized to supply electricity to the grid (Peng et al., 2012).

In the near future, when huge numbers of EVs will be used, they will take part in smart discharging and charging, which is an area of study that is starting to gain attention. Some solutions and models have been suggested for the scheduling challenge for charging and discharging of EVs (Galus and Andersson, 2008; Yao et al., 2013). Saber and Venayagamoorthy (2011) utilized PEVs and renewable energy sources to the fullest extent possible, taking into account the economic and emission goals while planning PEV usage. Hoehne and Chester (2016) put forth an ideal charging schedule, taking into account both standard and V2G PEV usage, to reduce carbon emissions. The authors concluded that using V2G during peak hours helps minimize carbon dioxide emissions. Ustun et al. (2013) examined the impact of PEVs on the power grid using three methods. PEVs can provide a way to replace fuel with domestic resources for energy independence, minimized carbon dioxide emissions, and lower fuel cost by developing advanced battery technologies. When compared with other technologies, Li-ion batteries have shown higher energy storage and power delivery capabilities, but they also have a far longer life in the deep-discharge cycling required for EV development (Keshan and Thornburg, 2016). Wei et al. (2022) studied the degrading characteristics of Li (NiMnCo)O_2 batteries under V2G applications and demonstrated that even if additional energy leads to cyclic degradation, V2G discharging reduces battery decay by 0.95% as compared to charging since it extends the battery's calendar life. Bhoir et al. (2021) evaluated the potential earnings for an auxiliary service provider using a fleet of EVs to offer various ancillary services on the power market in Li-ion batteries through a case study utilizing this battery concept. It demonstrates that the most profitable endeavor is to offer both peak shaving and frequency containment reserve. Hadi Amini et al. (2017) proposed fast-charging strategies for preventing or minimizing lithium plating. The charge profiles for both online and offline applications are obtained using the impedance tracking (IT) approach. When compared to current/constant voltage (CC-CV), the suggested solutions increased battery life by over 75%, with only a slight increase in the related charge time. Shargh et al. (2016) studied the Li-ion battery to reduce degradation through state-of-charge pre-conditioning strategies that allow an electric vehicle to participate in vehicle-to-grid operations during periods in which the vehicle is parked. In comparison to the reference standard charging approach,

the analytical results demonstrate that the proposed charging strategies do not accelerate battery degradation and can mitigate the entire aging process, starting at 7.3 26.7% for the first 100 days of operational life and gradually increasing to 8.6 12.3% for a year of continuous operation. Shazly et al. (2023) developed a double-stage method for distributing EV parking spaces with distributed renewable resources throughout the power distribution system. It takes into account the financial gains of parking lot investors as well as the operational technical limitations of distribution network operators. Singh et al. (2014) used a point estimate method (PEM) for Nataf transformation, and the joint probability density function (PDF) of wind speed related to different places was generated using marginal PDF, and the correlation matrix is available in most cases, which satisfy the service condition of Nataf transformation. Xie et al. (2024) suggested two-layer optimal dispatch systems to fully realize the promise of the EV demand response and address the issues caused by the integration of new energy vehicles into the power grid. The first approach is to evaluate the potential for an EV load demand response, and the second is to use the evaluation value of the EV response potential as the load adjustment range. These tactics are used in real-time, and the scheduling outcomes demonstrate the strategy's greater economic viability. Nourianfar and Abdi (2023) used an improved multi-objective exchange market algorithm to resolve the multi-objective dynamic economic emission dispatch problem in the presence of wind farms and EVs simultaneously. The performance of the suggested strategy and the efficacy of the suggested method are examined. The findings demonstrate that the addition of EVs lowered both the system's operating costs and emissions. Guo et al. (2021) presented a new multi-level optimal V2G scheduling approach to guarantee seamless operation and control from the V2G control center to the EV users, in addition to introducing a new EV economic dispatch optimization model to reduce the operating expenses of regional V2G systems. Furthermore, the viability of the suggested model suggested that extra load variations caused by large-scale vehicle fleets may be minimized through appropriate size regulation of the total EV battery capacity. Dynamic economic emission dispatch is simultaneously solved by Tawfak Al-Bahrani et al. (2020) on 30,000 electric vehicles during crest shaving and valley filling (CSVF) regions, while applying load demand management (LDM) under different actual equality and inequality operating power limitations. Zou et al. (2022) suggested a novel NSGA-II (NNSGA-II) to address dynamic economic emission dispatch with plug-in electric vehicles. This new method takes into account both the density and evenness of solutions by incorporating a rewarding coefficient into the crowding distance during density estimation.

Motivation: although implementation of EVs has limitations, with the development of technologies, infrastructures, and power grids, EVs will dominate the car market. In addition, with the depletion of fossil fuel supplies, the production and consumption of electric power can be resolved by considering renewable energy resources and EV technologies. Wind power is a renewable energy source that has drawn considerable attention. Their quick development has presented the electrical grid with additional difficulties. That is why large-scale deployment of EVs and renewable energy resources is inevitable in future microgrids. With the development of V2G applications, batteries can also be

FIGURE 1
Work flowchart of the proposed work.
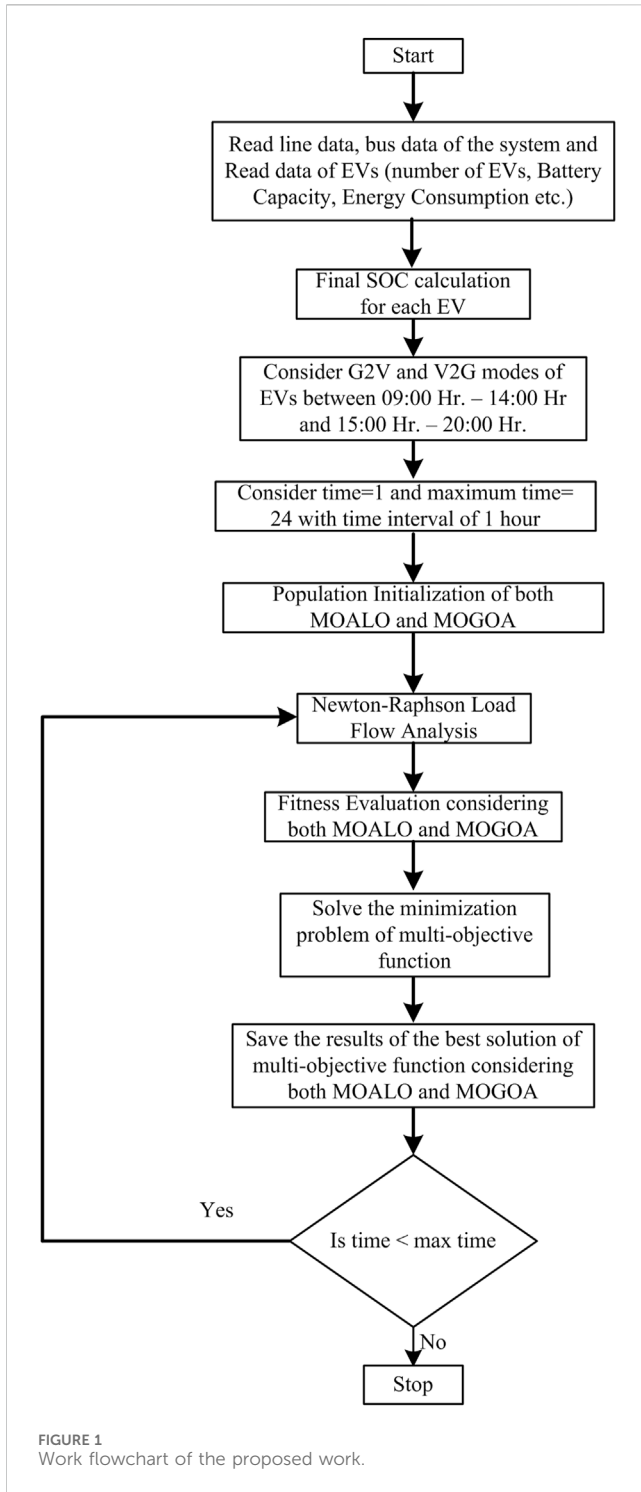
improved to act as an energy storage system (ESS), and thus, a certain number of V2G vehicles can act as a small power plant and reduce peak demand on the power grid. EVs can lead to sustainable development in the power distribution network. The EV industry is booming around the world, which may further impose much pressure on the existing network infrastructure. Therefore, there is lot of scope to verify the impact of EVs on the power system. This motivates the authors to work on the topic of EVs' impact on the power system operation.

Research gap: from the literature review, it is observed that EVs, at V2G and G2V modes of operation, can be used for valley filling and peak shaving, so in this paper, valley filling and peak shaving are achieved by implementing large-scale EVs during peak hours, as well as minimizing the generation cost and power loss of the system.

Novelty: we have tried to demonstrate the impact of a large scale of EVs on the power system cost and loss minimization based on a multi-objective problem. In addition, the demonstration on the peak load shaving and valley filling considering large-scale EVs in V2G and G2V modes has been analyzed in the proposed work.

The contribution of the work is summarized below:

- A 30-bus test is optimized using the MOGOA and MOALO to reduce the generation cost and loss of the system.
- Four different types of EVs are integrated into the system with different parameters and SOCs.
- During off-peak hours, all the EVs are set to charge, and during peak hours, all the EVs are set to discharge.
- This operation of V2G vehicles can reduce the power generation of the conventional power plants, which ultimately reduces the generation cost and power loss of the plant.

The rest of this paper is organized as follows: Section 2 shows the mathematical formulation of ED problems with several power constraints. Section 3 shows the algorithms for applying the MOGOA and MOALO with flowcharts as shown in Figure 1. The experimental results and discussions are provided in Section 4, and Section 5 shows the conclusion and future scope of the work.

2 Mathematical formulation

2.1 Objective functions

The curve for the generator cost can be obtained by the quadratic function. The equation for the total generation cost $F(P_G)$ can be written as (Sahoo et al., 2024) in Equation 1.

$$F(P_G) = \sum_{i=1}^{N} [a_i P_i^2 + b_i P_i + c_i].\tag{1}$$

Here, N is the number of thermal units; a_i, b_i, and c_i are the cost coefficients of the *ith* unit in \$/hr; and P_i is the active power output of the *ith* generator expressed in MW.

The resistances present in transmission lines and various pieces of equipment cause power loss in the system. Active power loss is given in Equation 2 (Bahrani and Patra, 2017):

$$P_L = \sum_{q=1}^{NL} G_{q(ij)} \left[V_i^2 + V_j^2 - 2V_i V_j \cos(\theta_i - \theta_j) \right],\tag{2}$$

where V_i and θ_i symbolize the voltage magnitude and voltage angle at bus *i*, respectively, $G_{q(ij)}$ represents the transfer conductance between bus *i* and bus *j*, and *NL* symbolizes the number of transmission lines.

The multi-objective-based proposed objective function can be utilized for minimization of loss in active power and generation cost. Thus, the objective function is as in Equation 3 (Sahoo et al., 2024):
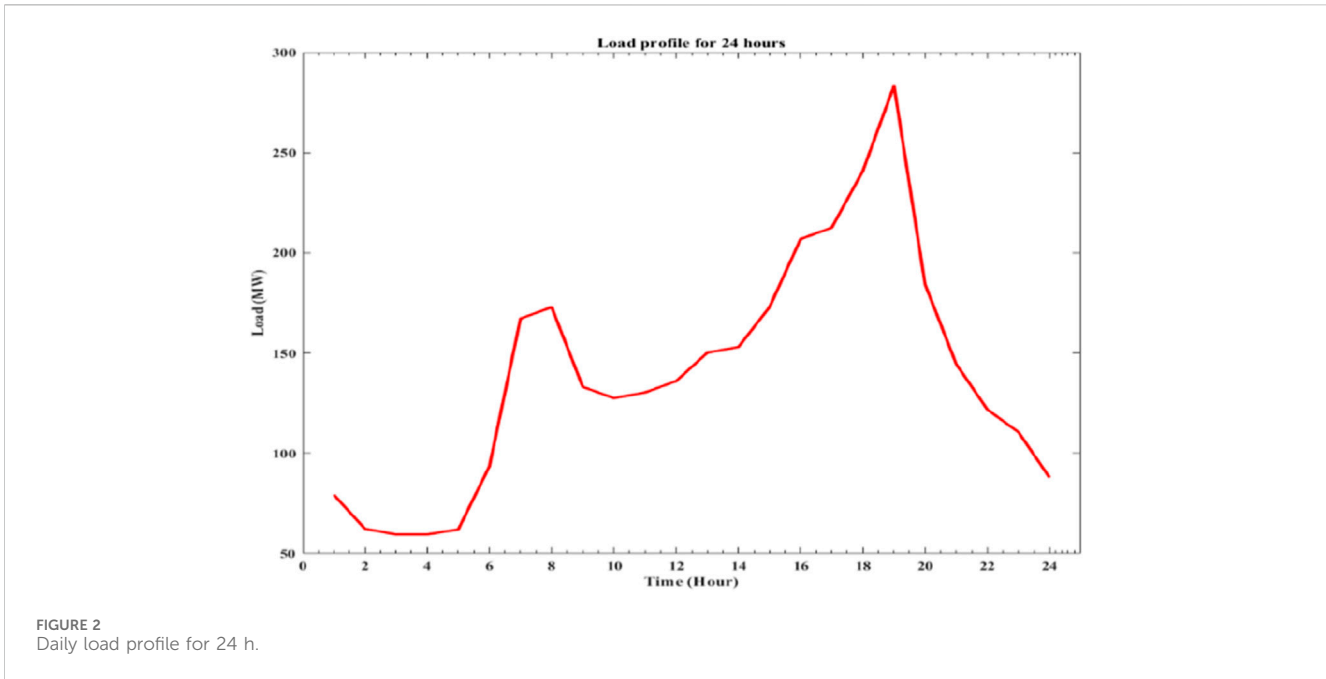
FIGURE 2
Daily load profile for 24 h.

TABLE 1 Daily load profile for 24 h.

Hr	P_D	Hr	P_D
01:00	79.3520	13:00	150.2020
02:00	62.3480	14:00	153.0360
03:00	59.5140	15:00	172.8740
04:00	59.5140	16:00	206.8820
05:00	62.0160	17:00	212.5500
06:00	93.5220	18:00	240.8900
07:00	167.2060	19:00	283.4000
08:00	172.8740	20:00	184.2100
09:00	133.1980	21:00	144.5340
10:00	127.5300	22:00	121.8620
11:00	130.3640	23:00	110.5620
12:00	136.0320	24:00	87.8540

TABLE 2 Comparison of the 30-bus system with and without the MOGOA.

Hr	Without optimization		With MOGOA	
	$F(P_G)$ ($/hr)	P_L (MW)	$F(P_G)$ ($/hr)	P_L (MW)
09:00	490.524	5.057816	349.491	3.20029
10:00	443.254	3.598746	331.427	2.97715
11:00	483.548	4.854874	342.924	2.88047
12:00	403.254	5.120659	358.387	3.31414
13:00	463.245	3.265487	384.589	1.58768
14:00	406.325	2.426587	386.41	1.85007
15:00	561.956	3.965485	452.029	2.07357
16:00	663.115	5.265787	549.898	3.67427
17:00	695.516	5.895134	567.262	4.03453
18:00	747.036	7.234897	656.941	5.81249
19:00	959.546	11.265478	803.015	10.0525
20:00	549.095	4.253951	479.605	2.75839
Total	6,866.414	62.2049	5,661.978	44.2155

$$Fobj_{\min} = \min\left(\sum \left(F(P_G) + P_L\right)\right). \tag{3}$$

The independent/control variables of the proposed work are P_G and V_G.

Here, P_G represents the active output power generation at PV buses, and V_G represents the voltage at generator buses. In addition, the dependent variable is V_L, and it represents the voltage value at PQ or load buses. The fitness function for the minimization problem is as in Equation 4:

$$f(x) = \frac{1}{(1 + Fobj_{min})}. \tag{4}$$

Here, $Fobj_{min}$ is the multi-objective function to be minimized (Nourianfar and Abdi, 2023).

2.2 Constraints

Constraints can be defined as a condition that a solution must satisfy in solving an optimization problem.

2.2.1 Power balance constraints

Considering the charging and discharging of EVs, the power balance equation of the system can be expressed as in Equation 5 (Tappeta et al., 2022):

$$\sum_{q=1}^{N} P_G + P_{V2G} = P_D + P_L + P_{G2V}. \tag{5}$$

TABLE 3 Power generation for 24 h using MOGOA.

Hr	G_1 (MW)	G_2 (MW)	G_3 (MW)	G_4 (MW)	G_5 (MW)	G_6 (MW)	P_G (MW)	P_D (MW)	P_L (MW)	$F(P_G)$ ($/hr)
01:00	58.0657	0	0	0	22.2503	0	80.3160	79.3520	0.964044	207.903
02:00	53.1255	0	0	0	10	0	63.1255	62.3480	0.784923	149.346
03:00	60.4454	0	0	0	0	0	60.4454	59.5140	0.931372	134.592
04:00	60.4382	0	0	0	0	0	60.4382	59.5140	0.927132	142.432
05:00	58.9359	0	0	0	10	0	68.9359	68.0160	0.919907	156.293
06:00	95.5573	0	0	0	0	0	95.5573	93.5220	2.04964	230.196
07:00	58.1932	39.0235	25.5549	24.0767	10	12	168.8483	167.2060	1.64529	445.581
08:00	71.5464	32.6574	22.5019	24.4668	10	13.7377	174.1901	172.8740	2.03614	455.191
09:00	120.016	0	0	16.3718	0	0	136.3881	133.1980	3.20029	349.491
10:00	115.897	0	0	14.61	0	0	130.5071	127.5300	2.97715	331.427
11:00	113.162	0	0	20.0678	0	0	133.2299	130.3640	2.88047	342.924
12:00	122.487	0	0	16.8558	0	0	139.3439	136.0320	3.31414	358.387
13:00	59.9112	32.8047	19.4131	17.6606	10	12	151.7897	150.2020	1.58768	384.589
14:00	67.6407	34.9552	20.0144	10.2728	10	12	154.8831	153.0360	1.85007	386.41
15:00	75.4348	31.5913	23.1672	22.7513	10	12	174.9446	172.8740	2.07357	452.029
16:00	110.035	31.8808	25.8612	20.5559	10.136	12.0772	210.5460	206.8820	3.67427	549.898
17:00	118.905	27.7449	23.3494	23.3094	10	13.266	216.5746	212.5500	4.03453	567.262
18:00	146.672	31.372	25.6022	21.0561	10	12	246.7025	240.8900	5.81249	656.941
19:00	191.621	46.8832	19.884	11.5011	10.3055	13.2576	293.4525	283.4000	10.0525	803.015
20:00	86.5733	39.268	22.715	16.4121	10	12	186.9684	184.2100	2.75839	479.605
21:00	113.763	0	33.5682	0	0	0	147.3315	144.5340	2.80755	380.054
22:00	125.242	0	0	0	0	0	125.2417	121.8620	3.37971	309.275
23:00	113.314	0	0	0	0	0	113.3138	110.5260	2.80223	274.817
24:00	89.6614	0	0	0	0	0	89.6614	87.8540	1.8216	209.47
Total									65.28509	8,757.128
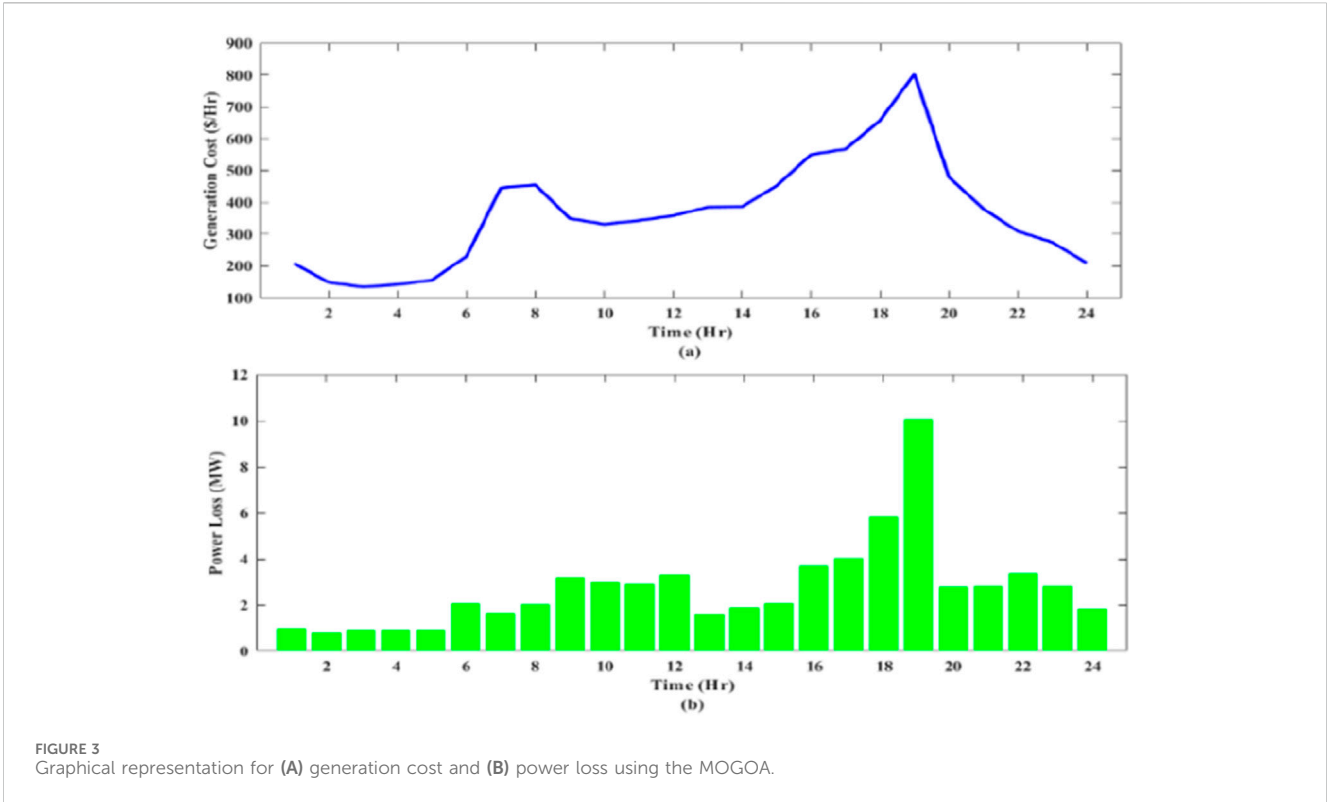
FIGURE 3
Graphical representation for **(A)** generation cost and **(B)** power loss using the MOGOA.
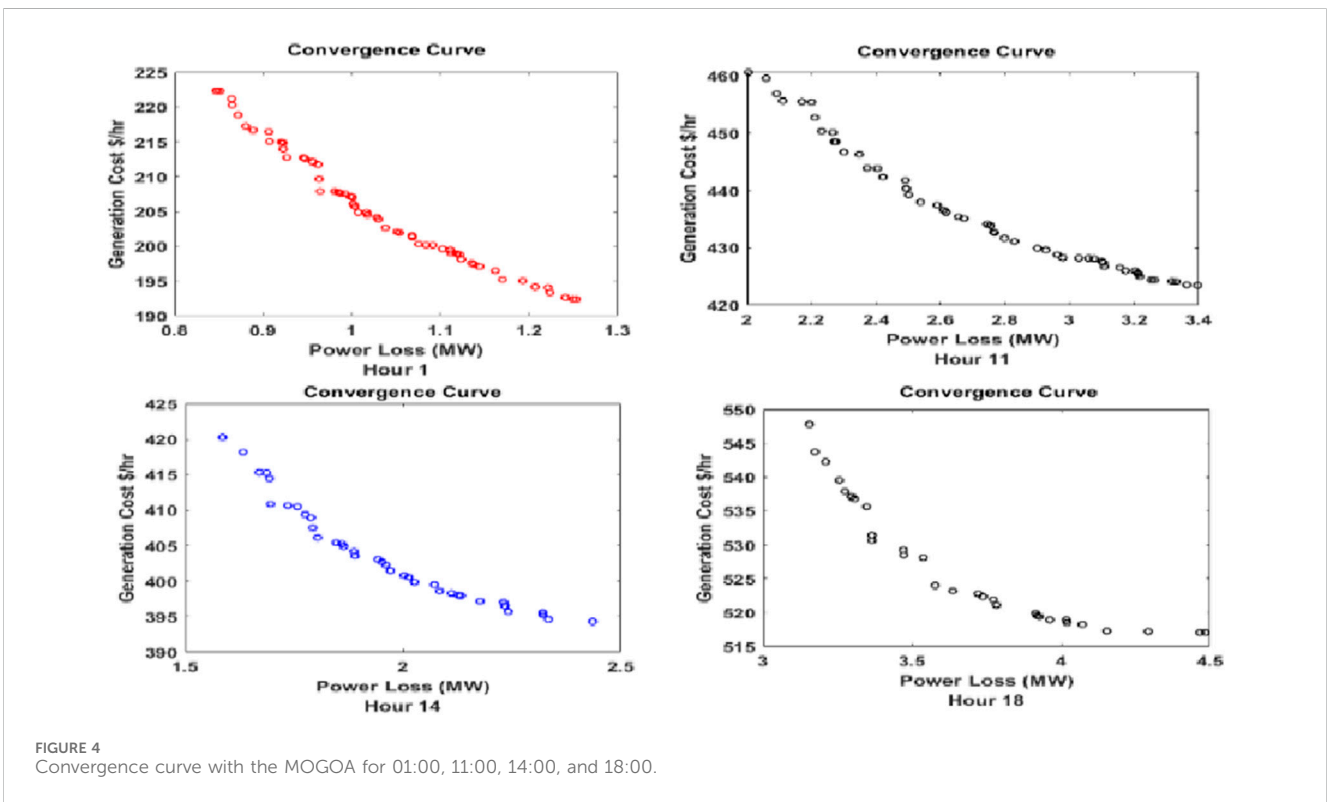
FIGURE 4
Convergence curve with the MOGOA for 01:00, 11:00, 14:00, and 18:00.

Here, P_{V2G} and P_{G2V} are the discharging power and charging load of PEVs, respectively, and P_D and P_L are the power load demand and active power loss in the system, respectively.

2.2.2 Equality constraints

It defines that power generation should be enough to supply load demand, including losses, to obtain the best value for the proposed

TABLE 4 Power generation for 24 h using MOALO.

Hr	G_1 (MW)	G_2 (MW)	G_3 (MW)	G_4 (MW)	G_5 (MW)	G_6 (MW)	P_G (MW)	P_D (MW)	P_L (MW)	$F(P_G)$ ($/hr)
01:00	58.2589	0	0	11.1317	10.9149	0	80.3055	79.3520	0.953494	202.18
02:00	52.9369	0	0	0	10.2001	0	63.1370	62.3480	0.798139	149.584
03:00	60.4431	0	0	0	0	0	60.4431	59.5140	0.929075	134.586
04:00	60.4322	0	0	0	0	0	60.4322	59.5140	0.927715	134.56
05:00	58.4354	0	0	0	10.4928	0	68.9282	68.0160	0.915118	163.907
06:00	71.0663	0	0	12.5753	11.2065	0	94.8481	93.5220	1.32608	240.019
07:00	59.3565	34.4063	23.4149	16.0462	15.2735	20.4338	168.9312	167.2060	1.73125	448.223
08:00	58.4972	36.0854	22.7562	22.6301	14.8641	19.8983	174.7313	172.8740	1.86326	468.413
09:00	83.682	0	15.6578	18.9431	16.6551	0	134.9380	133.1980	1.75105	346.063
10:00	81.8423	30.75	0	17.176	0	0	129.7682	127.5300	2.23823	317.445
11:00	71.9839	0	23.5117	17.2648	19.0204	0	131.7808	130.3640	1.41683	346.163
12:00	73.9987	43.7326	0	20.6334	0	0	138.3647	136.0320	2.33269	349.142
13:00	65.5956	24.8397	19.1263	13.038	15.72	13.9174	152.2372	150.2020	2.03515	387.308
14:00	61.7115	24.7929	26.2486	12.4047	14.4376	14.9384	154.5337	153.0360	1.5039	401.676
15:00	52.7322	40.9271	22.5615	17.4186	24.3705	16.5196	174.5295	172.8740	1.66503	474.684
16:00	85.1228	43.9815	22.5809	26.2104	16.2441	15.6811	209.8208	206.8820	2.94466	562.119
17:00	74.475	47.7816	28.386	25.5054	22.2332	16.7574	215.1386	212.5500	2.59859	596.735
18:00	107.4	46.328	32.0852	22.2937	20	16.8426	244.9491	240.8900	4.05908	677.334
19:00	103.03	59.9517	36.9537	34.2194	23.6988	30.1732	288.0272	283.4000	4.63289	855.381
20:00	65.9137	35.9099	27.3662	23.5017	16.0733	17.3702	186.1349	184.2100	1.92495	503.021
21:00	53.8509	29.7403	18.3744	16.7669	13.9975	13.4091	146.1390	144.5340	1.61484	374.026
22:00	59.6093	0	25.4934	24.8171	13.0677	0	122.9875	121.8620	1.13506	327.921
23:00	82.5606	0	0	18.4987	11.2204	0	112.2797	110.5260	1.76315	290.465
24:00	64.6332	0	0	11.764	12.6054	0	89.0025	87.8540	1.14854	226.107
Total									44.20877	8,977.062

optimization. The equations for power balance are in (Equations 6, 7).

$$P_{G_y} - P_{D_y} - V_y \sum_{a=1}^{N_B} V_a \left(G_{ya} \cos \theta_{ya} + B_{ya} \sin \theta_{ya} \right) = 0; \, y = 1, ..., N_B.$$

(6)

$$Q_{G_y} - Q_{D_y} - V_y \sum_{a=1}^{N_B} V_a \left(G_{ya} \cos \theta_{ya} - B_{ya} \cos \theta_{ya} \right) = 0; \, y = 1, ..., N_B.$$

(7)

Here, index P_{G_q} indicates the real power generation at the yth bus; P_{D_q} is the real power demand at the yth bus; V_y and V_a are the voltage magnitude at the yth and ath bus, respectively; and G_{ya} and B_{ya} are the conductance and susceptance of the yth and ath bus, respectively.

The inequality constraints are given in (Equations 8–11).

i. *Generator constraints:* it refers to the reactive power, active power, and voltage outputs in the system, which is bounded as follows (Jayabarathi et al., 2016):

$$V_{G_p}^{\min} \leq V_{G_p} \leq V_{G_p}^{\max}; \, p = 1, ..., N_G.$$

(8)

$$P_{G_p}^{\min} \leq P_{G_p} \leq P_{G_p}^{\max}; \, p = 1, ..., N_G.$$

(9)

Here, the indexes V_{Gp} and P_{Gp} indicate the magnitude of voltage and generation of real power, respectively, and the number of the generating unit is represented as N_G.

ii. *Security constraints:* the term "security constraints" refers to the restrictions on the load bus voltage and the line's maximum power flow rate. It can be formulated as follows (Jayabarathi et al., 2016):

$$V_{L_r}^{\min} \leq V_{L_r} \leq V_{L_r}^{\max}; \, r = 1, ..., N_L.$$
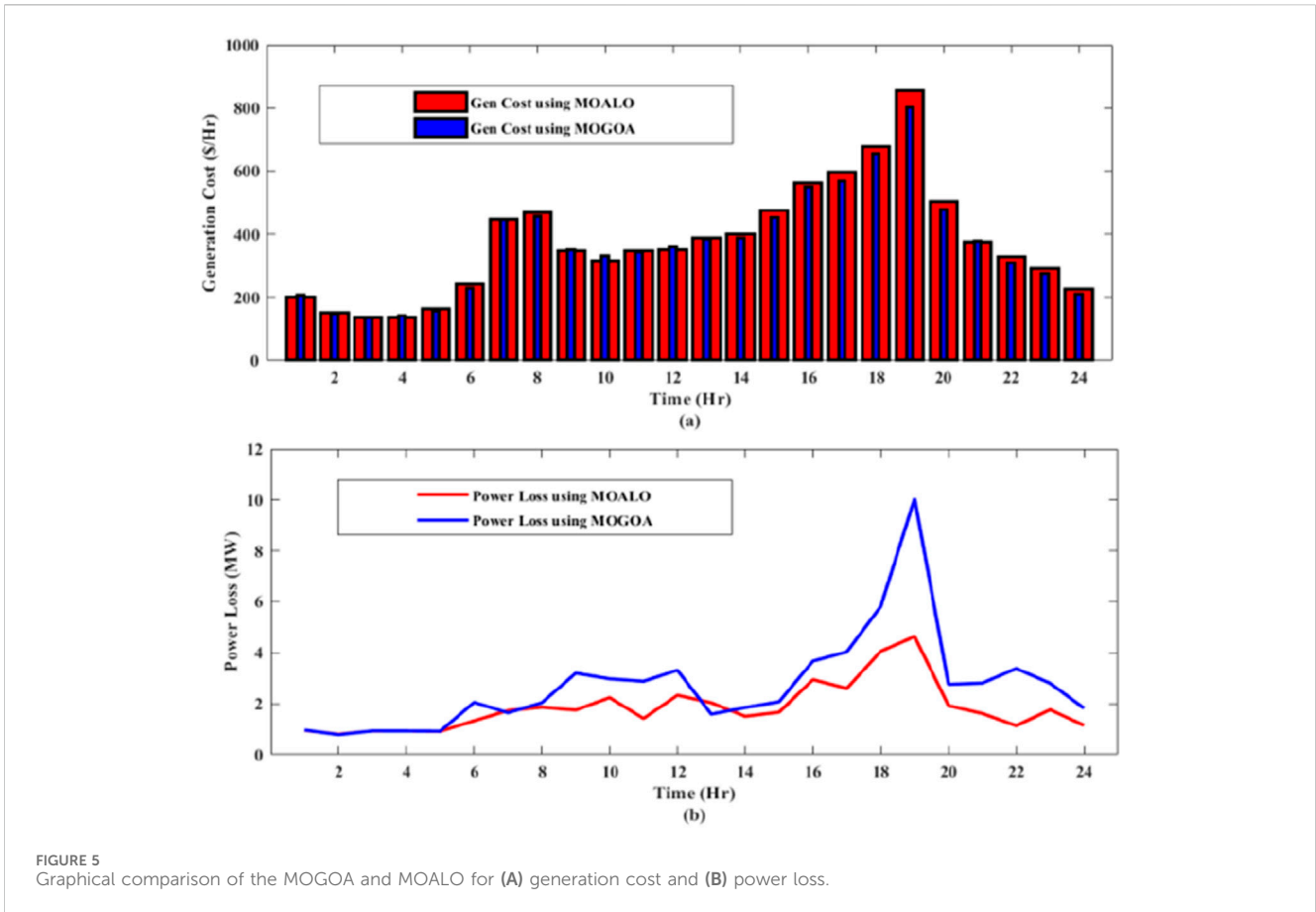
(10)

FIGURE 5
Graphical comparison of the MOGOA and MOALO for **(A)** generation cost and **(B)** power loss.

$$S_{L_n}^{\min} \leq S_{L_n}^{\max}; n = 1, ..., N_{BR}. \tag{11}$$

2.3 Single EV recharge energy

This section develops the energy consumption for charging an EV using the proposed probabilistic model in Shazly et al. (2023), such that the key determinants of how an EV charges, such as its battery capacity, operating condition, daily driving range, and other parameters, are taken into account.

According to statistics on EV driving behavior in Shazly et al. (2023), the daily miles that an EV travels, denoted as M_d, generally adheres to the lognormal distribution, in Equation 12.

$$M_d = e^{\left(\mu_m + \sigma_m \bullet N\right)}. \tag{12}$$

Here, the standard normal variate is given as N; μ_m and σ_m are the parameters for log-normal obtained from the mean and standard variation of M_d, represented as μ_{M_d} and σ_{M_d}, respectively (Shazly et al., 2023) as in Equation 13.

$$\begin{cases} \mu_m = \ln\left(\dfrac{\mu_{M_d}^2}{\sqrt{\mu_{M_d}^2 - \sigma_{M_d}^2}}\right) \\ \sigma_m = \sqrt{\ln\left(1 + \dfrac{\sigma_{M_d}^2}{\mu_{M_d}^2}\right)} \end{cases}. \tag{13}$$

Then, the maximum achievable driven distance, M_{dmax}, can be calculated as in Equation 14 (Shazly et al., 2023):

$$M_{d\max} = \frac{\beta}{E_m}. \tag{14}$$

Here, β is the battery capacity of each EV, and E_m denotes the energy consumption of the EVs.

The anticipated energy requirement of an electric vehicle based on the maximum distance traveled can be calculated as in Equation 15 (Shazly et al., 2023):

$$E_d = \begin{cases} \beta; & M_d \geq M_{d\max} \\ M_d E_m; & M_d \leq M_{d\max} \end{cases}. \tag{15}$$

The initial SOC is given as SOC_{ini}, and the final state of charge, SOC_f, can be expressed as in Equation 16 (Shazly et al., 2023):

$$SOC_f = SOC_{ini} - \frac{E_m \bullet d}{\beta} \times 100. \tag{16}$$

Here, "d" is the daily traveled distance of each vehicle.

The charging time of a single EV can be expressed as in Equation 17, (Shazly et al., 2023):

$$Charging\ time\ (hr) = \frac{Charge\ needed\ (kWh)}{Rate\ of\ charging\ (kW)}. \tag{17}$$
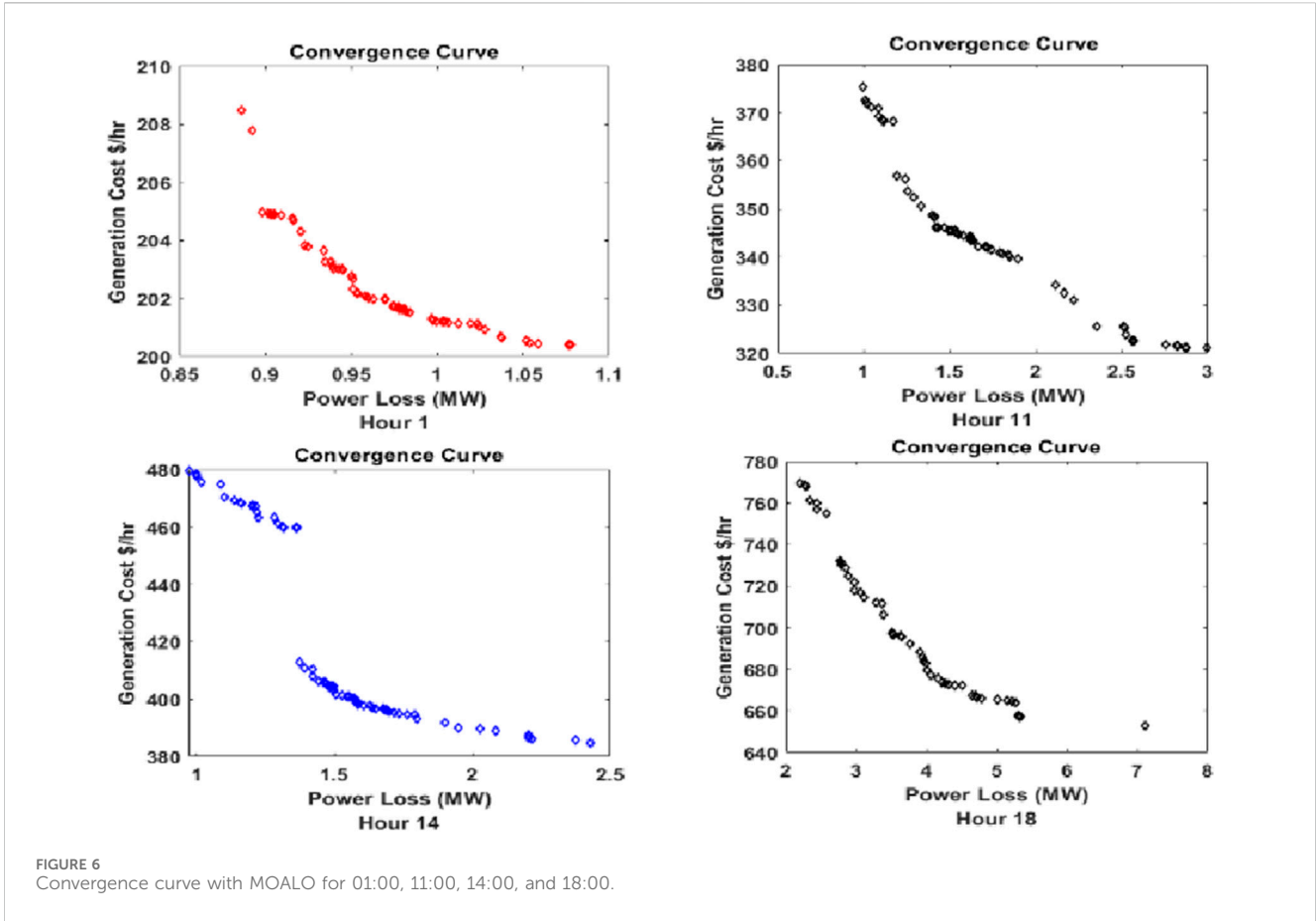
FIGURE 6
Convergence curve with MOALO for 01:00, 11:00, 14:00, and 18:00.

TABLE 5 Parameters of EV.

Types of vehicles	No. of vehicles	Energy consumption E_m (kWh/mile)	Battery capacity β (kWh)	Rate of charging (kW)	SOC_f
Micro car	20,800	0.3790	10	1.44	57.68
Economy car	3,500	0.4288	12	1.44	36.74
Mid-size Car	4,000	0.5740	16	1.44	42.47
Light truck/SUV	4,500	0.8180	21	7.68	46.75

TABLE 6 Time and energy required during the charging condition.

Types of vehicles	Energy required (kWh)	No. of vehicles	Total energy required (kWh)	Time required
Micro car	3.232	20,800	67.22	2.83
Economy car	4.4	3,500	15.4	3.85
Mid-size car	6.79	4,000	27.16	5.95
Light truck/SUV	9.8175	4,500	44.18	1.27

TABLE 7 Power generation during charging condition using the MOGOA.

Hr	G_1 (MW)	G_2 (MW)	G_3 (MW)	G_4 (MW)	G_5 (MW)	G_6 (MW)	P_G (MW)	P_{G2V} (MW)	P_D (MW)	P_L (MW)	$F(P_G)$ ($/hr)
09:00	95.9851	35.8705	19.8854	34.8926	10	17.0816	213.7151	75.3	133.1980	5.21714	571.004
10:00	92.711	39.6194	20.3045	33.1937	10	12	207.8285	75.3	127.5300	5.00246	549.702
11:00	71.9915	31.044	21.32	23.581	10.0719	12	170.0085	37.11	130.3640	2.53754	437.968
12:00	50.9405	29.933	25.6478	15.8467	10	13.5458	145.9138	8.56	136.0320	1.32177	377.756
13:00	61.8324	30.0053	24.5138	16.5696	10	13.449	156.3701	4.56	150.2020	1.61109	401.848
14:00	64.7149	33.4654	21.4414	16.1668	10	13.6088	159.3973	4.56	153.0360	1.80433	406.151

TABLE 8 Time and energy required during the discharging condition.

Types of vehicles	Energy required (kWh)	No. of vehicles	Total energy required (kWh)	Time required
Micro car	4.5	20,800	93.6	3.125
Economy car	5.52	3,500	19.32	3.84
Mid-size car	7.68	4,000	30.72	5.34
Light truck/SUV	10.5	4,500	47.25	1.36

TABLE 9 Power generation during the discharging condition using the MOGOA.

Hr	G_1 (MW)	G_2 (MW)	G_3 (MW)	G_4 (MW)	G_5 (MW)	G_6 (MW)	P_G (MW)	P_{V2G} (MW)	P_D (MW)	P_L (MW)	$F(P_G)$ ($/hr)
15:00	75.3405	33.9269	20.3178	17.6352	10	12	169.2204	5.75	172.8740	2.09949	429.609
16:00	111.234	30.1482	20.6216	20.7762	10	12	204.7804	5.75	206.8820	3.65143	527.956
17:00	90.8946	20	27.7355	12.536	10.0505	13.0475	174.2642	40.73	212.5500	2.4442	448.713
18:00	107.721	30.4821	28.8011	14.5306	10	12	203.5345	40.73	240.8900	3.37757	530.29
19:00	125.664	20	34.721	10	10	12	212.3848	75.47	283.4000	4.4652	568.047
20:00	80.6304	0	30.2083	0	0	0	110.8387	75.47	184.2100	2.10173	272.883

3 Multi-objective optimization and work flowchart

3.1 Grasshopper optimization algorithm

This technique copies the swarming nature of grasshoppers as a reference. The inspiration was obtained from how grasshoppers swarm on food locations. The algorithm proceedings show a similar function to that of the particle swarm optimization algorithm. The searching process includes exploration of random areas where food will most likely be available, as in the case of grasshoppers (Latif et al., 2021).

The grasshopper swarm's social interaction, gravitational pull, and wind advection are the three factors that make up the optimization. The positions of grasshoppers are theoretically predicted as in Equation 18:

$$X_P = S_P + G_P + A_P. \tag{18}$$

Here, X_P represents the pth grasshopper position, S_P represents the pth grasshopper social interaction, G_P is the gravitational force, and A_P is the wind advection. The social interaction between the grasshoppers is given as in Equations 19, 20:

$$S_P = \sum_{\substack{q=1 \\ q \neq 1}}^{M} s\left(\left|x_q\text{-}x_P\right|\right) \frac{(x_q\text{-}x_P)}{D_{pq}}. \tag{19}$$

$$s(y) = f e^{\frac{-y}{kk}} \text{-} e^{-y}. \tag{20}$$

The social force influencing the grasshopper is denoted as the function s in Equation 15, whereas f denotes the attraction's strength, y denotes the separation of the grasshopper, and kk is the attraction's length. Using the equation below, the grasshopper position can be implemented as in Equations 21, 22.

$$x_P^z = G\left(\sum_{q=1/q\neq 1}^{M} G \frac{x_{\max}^z - x_{\min}^z}{2} s\left(\left|x_q^z - x_P^z\right|\right) \frac{(x_q^z - x_P^z)}{D_{pq}^z}\right) + x_{gbest}^z. \tag{21}$$

$$G = G_{\max} - iter \frac{G_{\max} - G_{\min}}{iter_{\max}}. \tag{22}$$

Here, "G" is the optimization algorithm's parameter, "p" denotes the position of the zth variable, "D_{pq}^z" shows the distance between the zth variable's pth and qth position, and "x_{gbest}^z" denotes the global best of the zth variable (Latif et al., 2021).

FIGURE 7
Graphical comparison using the MOGOA with EV and without EV between 09:00 and 20:00 for **(A)** generation cost and **(B)** power loss.
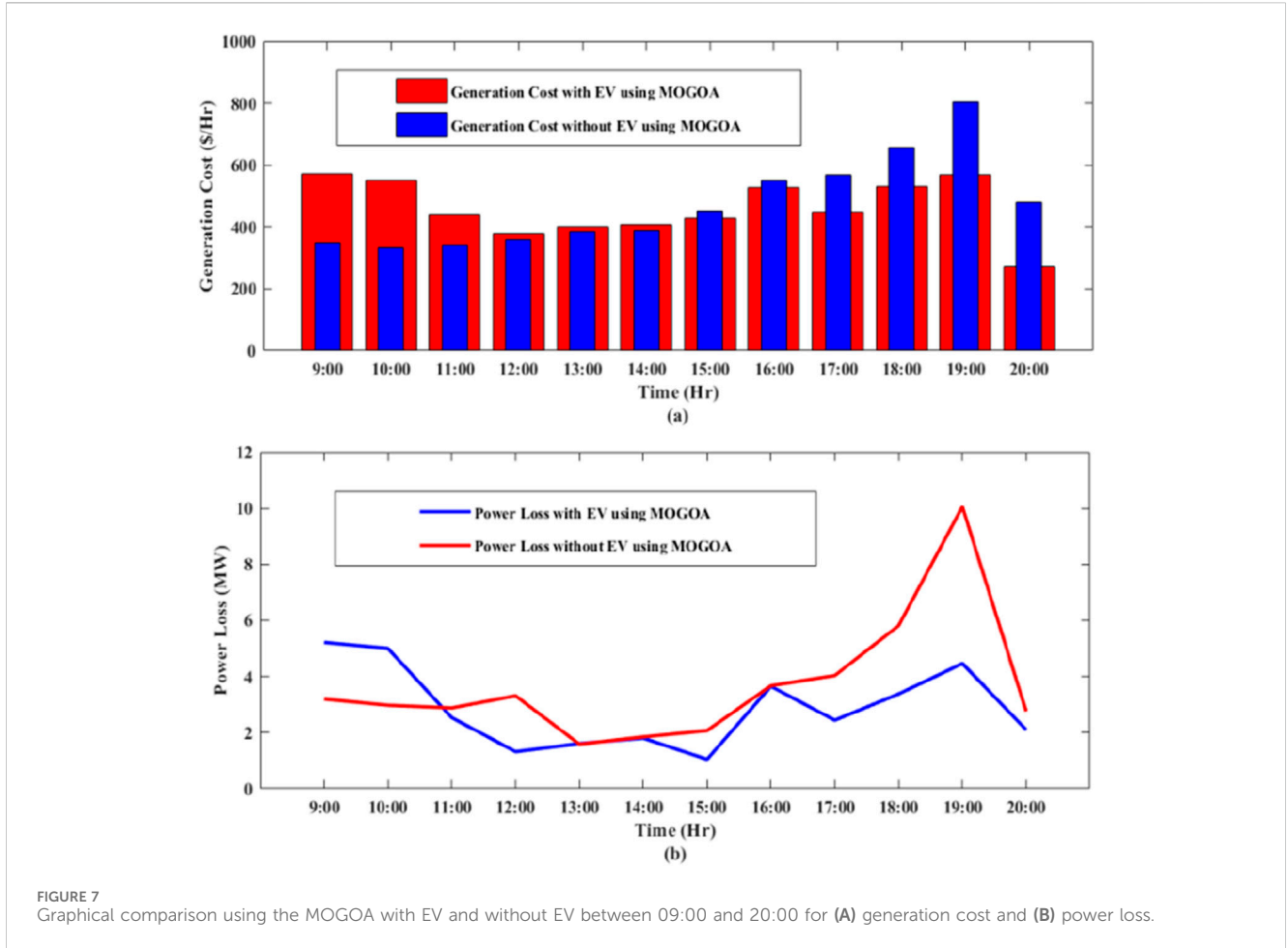
3.2 Ant-lion optimization

This optimization technique copies the hunting behavior of the ant lion, i.e., how they interact with their prey such as ants in nature. The MOALO was an extended edition of the ant lion optimizer (ALO). The operation of this optimization shares some similarity with the other population-based optimization techniques such as the MOPSO and MOGOA (Lalhmachhuana et al., 2024).

The algorithm of the multi-objective ant lion optimizer is as follows (Lalhmachhuana et al., 2024):

1. Initialize the population of the ant having random values.
2. The individual in the population is evaluated for objective function.
3. A random walk-around technique is used to explore the search space. It is given as in Equation 23.

$$X(y) = \begin{bmatrix} 0, cumsum\left(2r\left(y_1\right) - 1\right), \\ cumsum\left(2r\left(y_2\right) - 1\right)...., \\ cumsum\left(2r\left(y_n\right) - 1\right) \end{bmatrix}. \tag{23}$$

Here, r is a random value in the range 0–1, $cumsum$ is a term for calculating the cumulative sum, and y is the steps of iteration.

4. The ants are then normalized such that the position of the ants is maintained inside the search space, which is given as in Equation 24:

$$X_j^y = \frac{\left(X_j^y - a_j\right) \times \left(d_j^y - c_j^y\right)}{\left(b_j - a_j\right)} + c_j^y. \tag{24}$$

Here, X_j^y is the position of the ant, a_j is the minimum of the random walk around, b_j is the maximum of the random walk around, c_j^y is the minimum of the jth variable at the yth iteration, and d_j^y is the maximum of the jth variable at the yth iteration.

5. The ant lion population is not evaluated because they are assumed to be in the location of the ant position for the first iteration and relocate their position accordingly based on the position of the ants.
6. An elite ant lion also exists to follow the position of the ant regardless of their distance.
7. If only the ant lion is fitter than the elite, then the elite will be replaced by the ant lion.
8. Increasing the generation or iteration.
9. If the generation reaches its maximum, END the loop.

FIGURE 8
Convergence curve with the MOGOA integrating EV for 13:00, 14:00, 17:00, and 18:00.
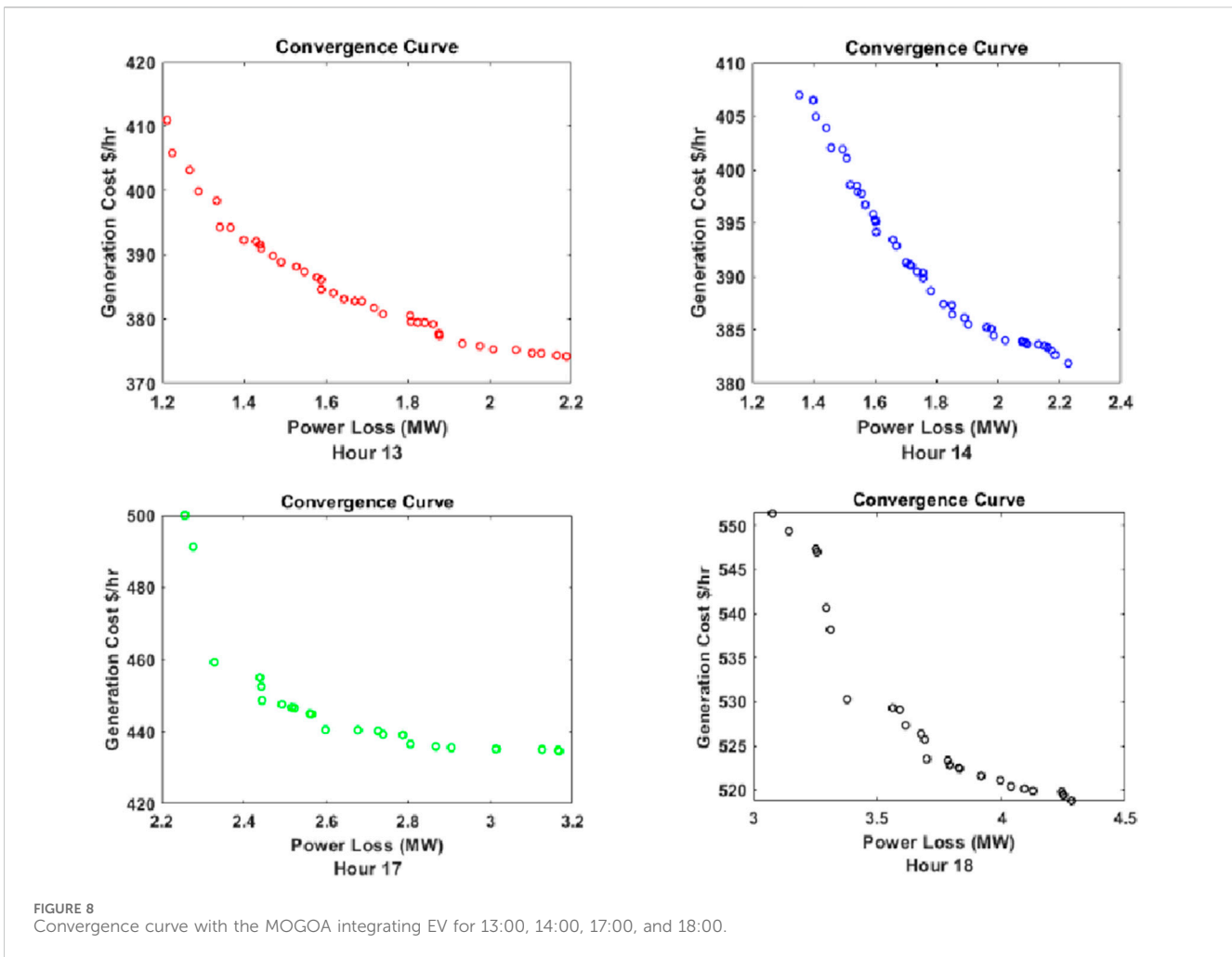
3.3 Work flowchart of the proposed work

The work flowchart is summarized below:

First, the line data and bus data are collected from the 30-bus test system. The information of EVs such as the number of EVs, battery capacity, and energy consumption is read. Then, Newton–Raphson load flow analysis is performed with and without considering EVs. The final SOC of each vehicle is calculated. Based on the different SOC_f, the EVs are set to G2V and V2G modes of operation between 09:00 to 14:00 and 15:00 to 20:00. Then, MOGOA and MOALO optimization techniques are used to minimize the multi-objective functions, and the results are saved accordingly.

4 Results and discussions

A total of six generator bus, 20 loads, and 41 transmission lines can be obtained in an IEEE 30-bus system. The generators buses are located at 1, 2, 13, 22, 23, and 27. The line data and bus data are taken from Singh et al. (2014). The boundary limits of all the constraints are also taken from Singh et al. (2014).

In this work, to demonstrate the key characteristics of the suggested MOGOA and MOALO with the fuzzy satisfaction

maximization approach, simulation results are provided and represented in an hourly basis.

4.1 Parameters of both the multi-objective optimization techniques are set as shown below

- Population size (Np) is set at 100.
- Random populations are generated by bus generator limits and bus voltage limits.
- Repository size (Nr) is set at 100.
- Maximum number of iterations is set at 100.

In addition, a daily load profile is generated using a scaling factor ranging from [0, 1] against the total active power load of 283.4 MW for the IEEE 30-bus test system, as shown in Figure 2.

In addition, according to the above load profile, the table for load demand is given in Table 1.

In this work, most vehicles are assumed to leave home at 09:00 and reach home at 20:00. Thus, much of the comparison of the data will be done between these intervals (09:00–20:00 Hr.).

TABLE 10 Power generation with EVs for the MOGOA for 24 h.

Hr	G_1 (MW)	G_2 (MW)	G_3 (MW)	G_4 (MW)	G_5 (MW)	G_6 (MW)	P_G (MW)	P_D (MW)	P_L (MW)	$F(P_G)$ ($/hr)
01:00	58.0657	0	0	0	22.2503	0	80.3160	79.3520	0.964044	207.903
02:00	53.1255	0	0	0	10	0	63.1255	62.3480	0.784923	149.346
03:00	60.4454	0	0	0	0	0	60.4454	59.5140	0.931372	134.592
04:00	60.4382	0	0	0	0	0	60.4382	59.5140	0.927132	142.432
05:00	58.9359	0	0	0	10	0	68.9359	68.0160	0.919907	156.293
06:00	95.5573	0	0	0	0	0	95.5573	93.5220	2.04964	230.196
07:00	58.1932	39.0235	25.5549	24.0767	10	12	168.8483	167.2060	1.64529	445.581
08:00	71.5464	32.6574	22.5019	24.4668	10	13.7377	174.1901	172.8740	2.03614	455.191
09:00	120.016	0	0	16.3718	0	0	213.7151	208.498	5.21714	571.004
10:00	115.897	0	0	14.61	0	0	207.8285	202.83	5.00246	549.702
11:00	113.162	0	0	20.0678	0	0	170.0085	167.474	2.53754	437.968
12:00	122.487	0	0	16.8558	0	0	145.9138	144.592	1.32177	377.756
13:00	59.9112	32.8047	19.4131	17.6606	10	12	156.3701	154.762	1.61109	401.848
14:00	67.6407	34.9552	20.0144	10.2728	10	12	159.3973	157.596	1.80433	406.151
15:00	75.3405	33.9269	20.3178	17.6352	10	12	174.9704	172.8740	1.04949	429.609
16:00	111.234	30.1482	20.6216	20.7762	10	12	210.5304	206.8820	3.65143	527.956
17:00	90.8946	20	27.7355	12.536	10.0505	13.0475	214.9942	212.5500	2.4442	448.713
18:00	107.721	30.4821	28.8011	14.5306	10	12	244.2645	240.8900	3.37757	530.29
19:00	125.664	20	34.721	10	10	12	287.8548	283.4000	4.4652	568.047
20:00	80.6304	0	30.2083	0	0	0	186.3087	184.2100	2.10173	272.883
21:00	113.763	0	33.5682	0	0	0	147.3315	144.5340	2.80755	380.054
22:00	125.242	0	0	0	0	0	125.2417	121.8620	3.37971	309.275
23:00	113.314	0	0	0	0	0	113.3138	110.5260	2.80223	274.817
24:00	89.6614	0	0	0	0	0	89.6614	87.8540	1.8216	209.47
Total									55.65349	8,617.077

TABLE 11 Power generation during the charging condition using MOALO.

Hr	G_1 (MW)	G_2 (MW)	G_3 (MW)	G_4 (MW)	G_5 (MW)	G_6 (MW)	P_G (MW)	P_{G2V} (MW)	P_D (MW)<	P_L (MW)	$F(P_G)$ ($/hr)
09:00	119.641	0	31.2865	35	26.8819	0	212.8095	75.3	133.1980	4.31164	611.003
10:00	86.2023	28.5608	21.0888	32.2971	21.1787	17.0061	205.3337	75.3	127.5300	2.51015	562.725
11:00	60.1869	28.0732	25.2174	26.165	16.4407	13.554	169.6373	37.11	130.3640	2.16633	453.921
12:00	82.0722	0	23.2068	22.7236	18.3257	0	146.3283	8.56	136.0320	1.73627	387.801
13:00	51.6191	29.3732	18.3893	17.5875	15	24.4234	156.3925	4.56	150.2020	1.63358	417.804
14:00	51.03	27.2502	29.0352	17.7182	18.3699	15.7504	159.1539	4.56	153.0360	1.55791	431.435

4.2 Case I: ED problems without EVs

Initially, the IEEE 30-bus test system is studied using Newton–Raphson load flow, without considering any optimization algorithm. The total power loss within the interval 09:00–20:00 in the IEEE 30-bus system is 62.2049 MW, and the generation cost is 6,866.414 $/hr.

Now, the proposed optimization technique, the multi-objective grasshopper optimization algorithm (MOGOA), is used. The two objective functions are optimized using the GOA and fuzzy

TABLE 12 Power generation during the discharging condition using MOALO.

Hr	G_1 (MW)	G_2 (MW)	G_3 (MW)	G_4 (MW)	G_5 (MW)	G_6 (MW)	P_G (MW)	P_{V2G} (MW)	P_D (MW)	P_L (MW)	$F(P_G)$ ($/hr)
15:00	58.5457	28.5833	25.8066	22.6847	13.89	19.2247	169.095	5.75	172.8740	1.61101	453.118
16:00	91.2882	27.2864	25.2308	18.2133	21.6017	19.2782	202.8987	5.75	206.8820	1.76971	547.871
17:00	96.4041	0	29.8632	27.6103	20.1813	0	174.0588	40.73	212.5500	2.24863	480.078
18:00	96.6909	30.0783	25.6079	19.4578	13.3899	17.1756	202.4004	40.73	240.8900	2.24338	536.182
19:00	118.051	0	34.0816	35	23.6722	0	210.7544	75.47	283.4000	2.82998	606.921
20:00	67.3252	0	18.9612	13.4132	11.0614	0	110.7015	75.47	184.2100	1.97093	274.416

TABLE 13 Power generation with EVs for MOALO for 24 h.

Hr	G_1 (MW)	G_2 (MW)	G_3 (MW)	G_4 (MW)	G_5 (MW)	G_6 (MW)	P_G (MW)	P_D (MW)	P_L (MW)	$F(P_G)$ ($/hr)
01:00	58.2589	0	0	11.1317	10.9149	0	80.3055	79.3520	0.953494	202.18
02:00	52.9369	0	0	0	10.2001	0	63.1370	62.3480	0.798139	149.584
03:00	60.4431	0	0	0	0	0	60.4431	59.5140	0.929075	134.586
04:00	60.4322	0	0	0	0	0	60.4322	59.5140	0.927715	134.56
05:00	58.4354	0	0	0	10.4928	0	68.9282	68.0160	0.915118	163.907
06:00	71.0663	0	0	12.5753	11.2065	0	94.8481	93.5220	1.32608	240.019
07:00	59.3565	34.4063	23.4149	16.0462	15.2735	20.4338	168.9312	167.2060	1.73125	448.223
08:00	58.4972	36.0854	22.7562	22.6301	14.8641	19.8983	174.7313	172.8740	1.86326	468.413
09:00	119.641	0	31.2865	35	26.8819	0	212.8099	208.498	4.31164	611.003
10:00	86.2023	28.5608	21.0888	32.2971	21.1787	17.0061	205.3337	202.83	2.51015	562.725
11:00	60.1869	28.0732	25.2174	26.165	16.4407	13.554	169.6373	167.474	2.16633	453.921
12:00	82.0722	0	23.2068	22.7236	18.3257	0	146.3283	144.592	1.73627	387.801
13:00	51.6191	29.3732	18.3893	17.5875	15	24.4234	156.3925	154.762	1.63358	417.804
14:00	51.03	27.2502	29.0352	17.7182	18.3699	15.7504	159.1539	157.596	1.55791	431.435
15:00	58.5457	28.5833	25.8066	22.6847	13.89	19.2247	174.845	172.8740	1.61101	453.118
16:00	91.2882	27.2864	25.2308	18.2133	21.6017	19.2782	208.6487	206.8820	1.76971	547.871
17:00	96.4041	0	29.8632	27.6103	20.1813	0	214.7888	212.5500	2.24863	480.078
18:00	96.6909	30.0783	25.6079	19.4578	13.3899	17.1756	243.1304	240.8900	2.24338	536.182
19:00	118.051	0	34.0816	35	23.6722	0	286.2244	283.4000	2.82998	606.921
20:00	67.3252	0	18.9612	13.4132	11.0614	0	186.1715	184.2100	1.97093	274.416
21:00	53.8509	29.7403	18.3744	16.7669	13.9975	13.4091	146.1390	144.5340	1.61484	374.026
22:00	59.6093	0	25.4934	24.8171	13.0677	0	122.9875	121.8620	1.13506	327.921
23:00	82.5606	0	0	18.4987	11.2204	0	112.2797	110.5260	1.76315	290.465
24:00	64.6332	0	0	11.764	12.6054	0	89.0025	87.8540	1.14854	226.107
Total									41.69524	8,923.529

satisfaction maximization approach. Comparison between the two systems is shown in Table 2.

Table 2 shows that the proposed algorithm already improves the generation cost and power loss of the system. Table 3 shows the complete power generation, generation cost, and power loss of the system for 24 h.

As given in Table 3, for hour 1, the load demand (P_D) is 79.3520 MW. In order to meet the load demand, the power

FIGURE 9
Graphical comparison with EVs and without EVs using MOALO between 09:00 and 20:00 for **(A)** generation cost and **(B)** power loss.
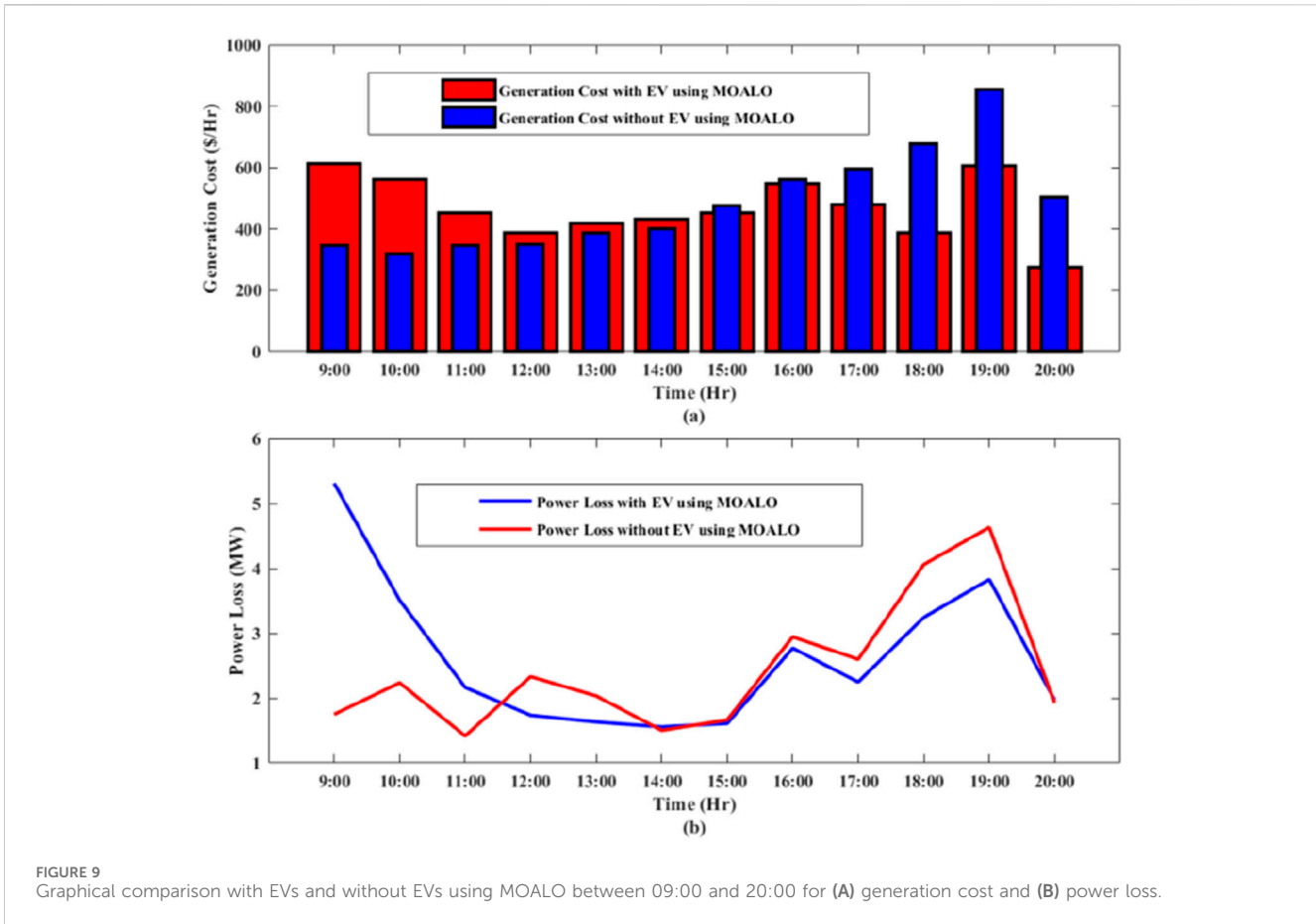
generated (P_G) at this particular hour is 80.3160 MW, which is the sum of the power generated by the six generators (G_1–G_6). Active power loss (P_L) is observed to be 0.964044 MW, and the total cost of power generation is 207.903 $/hr. The power generated can be observed for each hour and cost of power generation. It can be seen that the total generation cost and power loss for 24 h are 8,757.128 $/hr and 65.28509 MW, respectively. Figure 3 shows the graphical representations for the cost and loss using the MOGOA. Figure 4 shows some selected convergence curves for 24 h due to limitations of the number of figures.

Figure 4 shows the convergence curve for 01:00, 11:00, 14:00, and 18:00, respectively. Due to limitations of number of figures, convergence for all hours cannot be shown. So these hours are randomly selected. It should be noted that in some hours, there are few solutions. This is because the load demand is low during these hours, and only the slack bus is assumed to be generating power, and thus, minimum solutions can be seen during these convergences. This can also be seen in future cases. Now, another algorithm, called MOALO, is used to observe the performance of the objective functions, with the same parameters set as those of the MOGOA.

Table 4 shows the complete power generation, generation cost, and power loss of the system for 24 h. For 01:00, the load demand (P_D) is 79.3520 MW. In order to meet the load demand, the power generated (P_G) at this particular hour is 80.3055 MW, which is the sum of the power generated by the six generators (G_1–G_6). Active power loss (P_L) is observed to be 0.953494 MW, and the total cost of power generation is 202.18 $/hr. The rest of the power generations can be observed for each hour. In addition, it can be observed that the total generation cost and power loss for 24 h are 8,977.062 $/hr and 44.20877 MW, respectively. If we compare the multi-objective function of the MOGOA and MOALO, it is observed that the MOGOA performs better at minimizing the generation cost, while MOALO performs better at minimizing the power loss.

From Figure 5, it is clear that both the MOGOA and MOALO have better performances for the multi-objective functions compared to the others. It is clear that the MOGOA is better at minimizing the generation cost, while MOALO is better at minimizing power loss of the system. The convergence curve for MOALO can be seen in Figure 6. As mentioned before, due to limitations of the number of figures, some selected hours are shown.

4.3 Case II: ED problems with G2V and V2G

As shown in Table 5, a total number of 32,800 EVs is considered. In addition, for this case, most vehicles are assumed to leave home at 09:00 and leave their workplace at 20:00, so all the EVs are charging and discharging between these hours. The daily travel distance is assumed to be between 8 and 12 miles for all types of EVs. Four types

FIGURE 10
Convergence curve with MOALO integrating EV for 13:00, 14:00, 17:00, and 18:00.
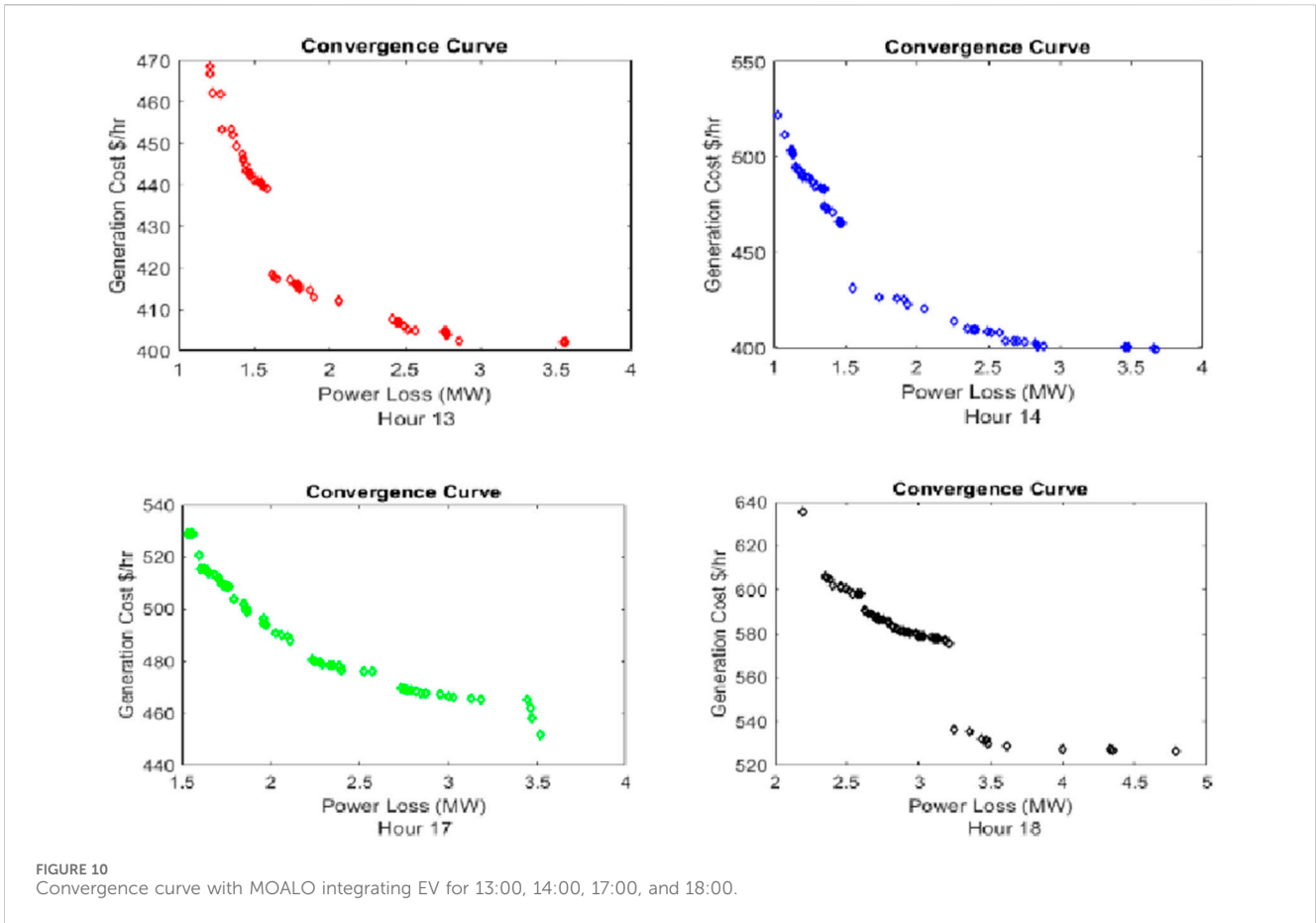
of EVs are considered, and the parameters of each type of EVs are shown in Table 5. The final SOC_f is calculated using Equation 16, and the calculated values are shown in the last column of Table 6. The energy consumption and battery capacity of each EV are taken from Shazly et al. (2023), while the total number of vehicles has been limited to meet the system demand. The number of micro cars is assumed to be highest as it is the most affordable by the common users. The economy cars, mid-size cars, and light trucks/SUVs are used for public and goods transportation and assumed to be approximately 3,500–4,500.

4.4 For charging condition using the MOGOA:

During 09:00 to 14:00, all EVs are set to the charging mode since it is the off-peak period. SOC_f is the state of charge that each vehicle is having when they reach their workplace at 09:00 (9 a.m.). If all vehicles are set to charging at 90%, then the amount of time required for each vehicle to reach 90% SOC is calculated using Equation 17 and shown in Table 6. P_{G2V} is the amount of energy required to charge EV, so it will be considered part of the load in the power balance constraint. This P_{G2V} will be randomly distributed to four buses, which produce the minimum values for the objective functions. During the charging condition, since there is extra energy required, the conventional power needs to produce more power to satisfy the power demand as well as the amount of energy

for charging EVs. So the power balance constraint can be written as in Equation 25:

$$P_G = P_D + P_L + P_{G2V}. \tag{25}$$

As shown in Table 3, at 09:00, the generation cost without EVs is 349.491 \$/hr. When EVs are set to charging, the power generated (P_G) has to satisfy the load demand (P_D) as well as the charging load (P_{G2V}), so higher power is generated during this period. Thus, the generation cost with EVs increased to 571.004 \$/hr, and the power loss will also be increased from 3.20029 MW to 5.21714 MW at this particular hour, as shown in Table 7. Thus, the generation cost and active power loss are higher in the presence of EVs within these hours.

4.5 For discharging condition using the MOGOA

During 15:00 to 20:00, all EVs are set to the discharging mode as it approaches the peak load hours. Final state of charge (SOC_f) for all the vehicles at 15:00 is 90%. Micro cars are set to discharge 45%, economy cars are set to discharge 46%, mid-size cars are set to discharge 48%, and light truck/SUVs are set to discharge 50%. Then, the time required for V2G is calculated using Equation 17 and shown in Table 8. P_{V2G} is the stored power discharged by the EVs from their battery to the grid, preferably during peak hours, so as to reduce power generation as well as peak demand. The discharged

TABLE 14 Comparison of the MOGOA with MOALO for 24 h with EVs.

Hr	With MOGOA		With MOALO	
	$F(P_G)$ ($/hr)	P_L (MW)	$F(P_G)$ ($/hr)	P_L (MW)
01:00	207.903	0.964044	202.18	0.953494
02:00	149.346	0.784923	149.584	0.798139
03:00	134.592	0.931372	134.586	0.929075
04:00	142.432	0.927132	134.56	0.927715
05:00	156.293	0.919907	163.907	0.915118
06:00	230.196	2.04964	240.019	1.32608
07:00	445.581	1.64529	448.223	1.73125
08:00	455.191	2.03614	468.413	1.86326
09:00	571.004	5.21714	611.003	4.31164
10:00	549.702	5.00246	562.725	2.51015
11:00	437.968	2.53754	453.921	2.16633
12:00	377.756	1.32177	387.801	1.73627
13:00	401.848	1.61109	417.804	1.63358
14:00	406.151	1.80433	431.435	1.55791
15:00	429.609	1.04949	453.118	1.61101
16:00	527.956	3.65143	547.871	1.76971
17:00	448.713	2.4442	480.078	2.24863
18:00	530.29	3.37757	536.182	2.24338
19:00	568.047	4.4652	606.921	2.82998
20:00	272.883	2.10173	274.416	1.97093
21:00	380.054	2.80755	374.026	1.61484
22:00	309.275	3.37971	327.921	1.13506
23:00	274.817	2.80223	290.465	1.76315
24:00	209.47	1.8216	226.107	1.14854
Total	8,617.077	55.65349	8,923.529	41.69524

powers are again randomly distributed to four buses of the system, which also produce the minimum values for the objective functions. Since EVs act as a power plant during this period, the power generated by the conventional power will be reduced. Then, the power balance constraint for discharging can be written as in Equation 26:

$$P_G + P_{V2G} = P_D + P_L. \tag{26}$$

The power generation during the discharging condition with the MOGOA (15:00 to 20:00) is shown in Table 9, with power discharged shown for each hour. At 15:00, the power demand (P_D) is 172.8740 MW, and in to order satisfy this load demand, the power generated (P_G) is 169.2204 MW, which is aided by the discharged power (P_{V2G}) of 5.75 MW, and thus, the generation cost is 429.609 $/hr.

As seen from Table 3, at 15:00, the power generation cost without EVs is 452.029 $/hr. When the EVs are set to discharging, the load demand (P_D) will be satisfied by the power generated ((P_G) by the conventional power plant as well as the discharged power (P_{V2G}), so power generation cost is reduced to 429.609 $/hr. In addition, at 15:00, power loss without EVs is 2.07357 MW. When EVs are set to discharge, energy is also supplied by the EVs, so power loss is reduced to 1.04949 MW, as shown in Table 9. Thus, generation cost and power loss will be reduced due to EVs during this period.

Figure 7 shows the comparison of generation cost and power loss for case I and case II for charging and discharging conditions (09:00 to 20:00) using the MOGOA. Figure 8 shows the convergence curve for four random hours between 09:00 to 20:00.

From Figure 7; Table 7; Table 9, it can be seen that the cost and loss are increased during the charging mode (i.e., 09:00–14:00), and during the discharging mode (i.e., 15:00–20:00), the cost and loss are reduced. Thus, peak shaving and valley filling can be observed in the presence of EVs. As shown in Table 10, the total generation cost for the MOGOA with EVs is 8,617.077 $/hr, and the total active power loss is 55.65349 MW.

Whereas in Table 3, the total generation cost for the MOGOA without EVs is 8,757.128 $/hr, and total active power loss of the system is 65.28509 MW. Thus, the difference is 140.051 $/hr for the power generation cost and 9.6316 MW for active power loss. Therefore, it can be concluded that the implementation of G2V and V2G in the system can help reduce the cost of the power generation and improves loss.

Now, MOALO is used to optimize the charging and discharging conditions and observe the variations in power generations as well as the objective functions during these hours.

4.6 For charging condition using MOALO

Table 11 shows the power generation cost for charging during 09:00 to 14:00. From Table 4, it can be seen that at 09:00, the generation cost without EVs is 346.063 $/hr. When EVs are set to charging, the generation cost at that particular hour increased to 611.003 $/hr, as seen from Table 11. The power loss increased from 1.75105 MW to 5.31164 MW, as observed on comparing Table 4 and Table 11. Thus, generation cost and power loss are high during this period with EVs.

4.7 For discharging condition using MOALO

During 15:00 to 20:00, all EVs are set to the discharging mode as it approaches the peak load hours. The final state of charge (SOC_f) for all the vehicles at 15:00 is 90%. Micro cars are set to discharge 45%, economy cars are set to discharge 46%, mid-size cars are set to discharge 48%, and light truck/SUVs are set to discharge 50%. Then, the time required for V2G is calculated using Equation 17 and shown in Table 12.

Table 12 shows discharging of EVs during 15:00 to 20:00. As shown in Table 4, during 15:00, the cost of generation without EVs is 474.684 $/hr. When EVs are set to discharging, the cost of
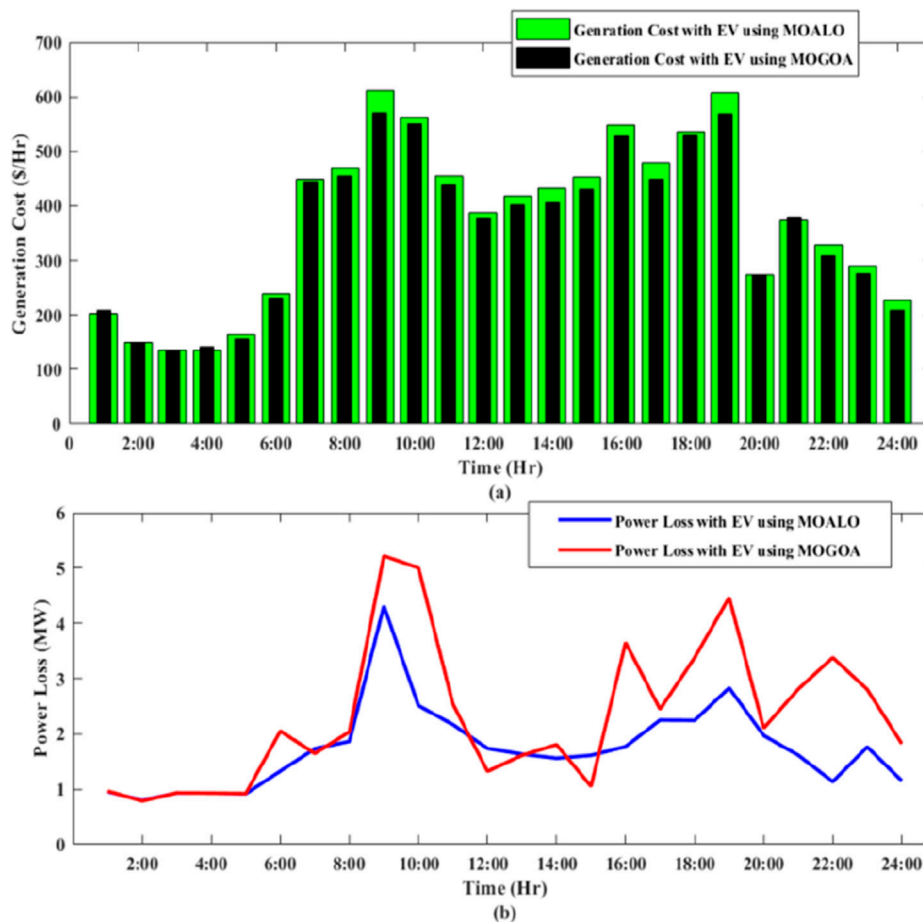
FIGURE 11
Graphical comparison of the MOGOA and MOALO for **(A)** generation cost and **(B)** power loss.

generation reduced to 453.118 $/hr, as observed in Table 12. Power loss without EVs at 15:00 is 1.66503 MW, and when EVs are discharged, power loss reduced to 1.61101 MW. Thus, generation cost and power loss are reduced in the presence of EVs.

MOALO is used with the same parameters as the MOGOA, with the same EV parameters as in Table 6 for charging condition and those in Table 8 for discharging condition. Table 11 shows the power generation for 09:00 to 14:00 with the EV load demand for each hour, and generation cost is high during these hours. Figure 9 shows the comparison of generation cost and power loss with and without EVs.

It can be seen that EVs can be used for peak shaving and valley filling while analyzing the effect on the objective functions with MOALO, while Figure 10 shows the convergence curve for MOALO with EVs for some selected hours due to limitations of space.

From Table 4, the total loss and cost for MOALO without EVs are 8,977.062 $/hr and 44.20877 MW, respectively. From Table 13, the total loss and cost for MOALO with EVs are 8,923.529 $/hr and 41.69524 MW, respectively. The difference for cost is 53.533 $/hr and for loss is 2.51353 MW. It is clear that the total loss and cost of

the system decrease when EVs are implemented between 09:00 and 20:00, and thus, it validates the optimization results using the MOGOA.

Below are the comparisons for the MOGOA and MOALO with EVs for 24 h. The comparison of the cost and loss for the two optimizing techniques is given in Table 14 below.

From the table above, it is clear that for the two algorithms, the loss and cost of the system decrease after implementing G2V and V2G. However, the two algorithms outperform the other at minimizing the objective functions. The total generation cost for the MOGOA is 8,617.077 $/hr, whereas for MOALO, it is 8,923.529 $/hr. In addition, the total power loss for the MOGOA is 55.65349 MW, whereas for MOALO, it is only 41.69524 MW.

It is clear that the MOGOA minimizes the generation cost better, while MOALO minimizes the power loss of the system better. The graphical comparison for generation cost and power loss between the MOGOA and MOALO during charging and discharging hours can be observed below. As shown in Figure 11A, the generation cost is lower for the MOGOA almost at all the hours, but as shown in Figure 11B, the power loss is much lower for MOALO at almost all of the hours.

5 Conclusion and future scope

5.1 Conclusion

In this work, the IEEE 30-bus system is used to analyze the economic dispatch (ED) problems with and without EVs. Four types of EVs with different parameters are used, and the final state of charge of each vehicle is calculated, along with the energy required and time of charging. Then, MOALO is used to optimize the objective functions with both cases without EVs and with EVs. EVs are set to charging from 09:00 to 14:00 and are set to discharging from 15:00 to 20:00. After implementing EVs to the system, it can be observed that the total generation cost and power loss of the system decrease due to V2G power discharging. In addition, EVs provide an alternative method for dealing with peak load, while filling the off-peak hours effectively. If the number of EVs is large enough, the V2G system can replace other peak shaving and valley filling techniques completely. On comparing the MOGOA and MOALO algorithms, the MOGOA excels at minimizing the generation cost, while MOALO excels at minimizing the power loss of the system.

5.2 Future scope

The thorough analysis of EVs' performance in the presence of renewable energy sources may further improve the power system's operation. The studies of carbon emission reduction can also be performed in the future.

5.3 Real-time application

The proposed work can be applied in real-time where a huge number of EVs is ready to participate in the G2V/V2G coordinated approach. The utilization of power electronics-based converters is also essential in real-time application during EV integration in the system.

Data availability statement

The original contributions presented in the study are included in the article/Supplementary Material; further inquiries can be directed to the corresponding authors.

Author contributions

DH: writing–review and editing and writing–original draft. SDe: writing–review and editing and writing–original draft. SDa: writing–review and editing and writing–original draft. KS: writing–review and editing and writing–original draft. UC: writing–review and editing and writing–original draft. TU: writing–review and editing and writing–original draft.

Funding

Conflict of interest

The authors declare that the research was conducted in the absence of any commercial or financial relationships that could be construed as a potential conflict of interest.

Publisher's note

All claims expressed in this article are solely those of the authors and do not necessarily represent those of their affiliated organizations, or those of the publisher, the editors, and the reviewers. Any product that may be evaluated in this article, or claim that may be made by its manufacturer, is not guaranteed or endorsed by the publisher.

References

Bahrani, L. T. A., and Patra, J. C. (2017). Orthogonal PSO algorithm for economic dispatch of thermal generating units under various power constraints in smart power grid. *Appl. Soft Comput.* 58, 401–426. doi:10.1016/j.asoc.2017.04.059

Bhoir, S., Caliandro, P., and Brivio, C. (2021). Impact of V2G service provision on battery life. *J. Energy Storage* 44, 103178. doi:10.1016/j.est.2021.103178

Chatuanramtharnghaka, B., Deb, S., and Datta, S. (2021). "Multi-objective based congestion management considering generation rescheduling and cost minimization using multi-verse optimizer," in *2021 1st international conference on power electronics and energy (ICPEE), bhubaneswar, India*, 1–6.

Chiang, C. L. (2005). Improved genetic algorithm for power economic dispatch of units with valve-point effects and multiple fuels. *IEEE Trans. Power Syst.* 20 (4), 1690–1699. doi:10.1109/tpwrs.2005.857924

Dey, P. P., Das, D. C., Latif, A., Hussain, S. M. S., and Ustun, T. S. (2020). Active power management of virtual power plant under penetration of central receiver solar thermal-wind using butterfly optimization technique. *Sustainability* 12, 6979. doi:10.3390/su12176979

Galus, M. D., and Andersson, G. (2008). "Demand management of grid connected plug-in hybrid electric vehicles (PHEV)," in *Proc. IEEE energy 2030 conf*, 1–8.

Guo, S., Qiu, Z., Xiao, C., Liao, H., Huang, Y., Lei, T., et al. (2021). Amulti-level vehicle-to-grid optimal scheduling approach with EV economic dispatching model. *Energy Rep.* 7, 22–37. doi:10.1016/j.egyr.2021.10.058

Hadi Amini, M., Parsa Moghaddam, M., and Karabasoglu, O. (2017). Simultaneous allocation of electric vehicles' parking lots and distributed renewable resources in smart power distribution networks. *Sustain. Cities Soc.* 28, 332–342. doi:10.1016/j.scs.2016.10.006

Hajimiragha, A., Cañizares, C. A., Fowler, M. W., and Elkamel, A. (2010). Optimal transition to plug-in hybrid electric vehicles in Ontario, Canada, considering the electricity-grid limitations. *IEEE Trans. Ind. Electron.* 57 (2), 690–701. doi:10.1109/tie.2009.2025711

Han, S., Han, H., and Sezaki, K. (2010a). "Design of an optimal aggregator for vehicle-to-grid regulation service," in *Presented at the IEEE power energy soc. Conf. Innovative smart grid technol* (Gaithersburg, MD).

Han, S., Han, H., and Sezaki, K. (2010b). Development of an optimal vehicle-to-grid aggregator for frequency regulation. *IEEE Trans. Smart Grid* 1 (1), 65–72. doi:10.1109/tsg.2010.2045163

Hoehne, C. G., and Chester, M. V. (2016). Optimizing plug-in electric vehicle and vehicle-to-grid charge scheduling to minimize carbon emissions. *Energy* 115, 646–657. doi:10.1016/j.energy.2016.09.057

Hussain, S. M. S., Aftab, M. A., Ali, I., and Ustun, T. S. (2020). IEC 61850 based energy management system using plug-in electric vehicles and distributed generators during emergencies. *Int. J. Electr. Power and Energy Syst.* 119, 105873. doi:10.1016/j.ijepes.2020.105873

Jayabarathi, T., Raghunathan, T., Adarsh, B., and Suganthan, P. N. (2016). Economic dispatch using hybrid grey wolf optimizer. *Energy* 111, 630–641. doi:10.1016/j.energy.2016.05.105

Kempton, W., and Letendre, S. E. (1997). Electric vehicles as a new power source for electric utilities. *Res* 2 (3), 157–175. doi:10.1016/s1361-9209(97)00001-1

Kempton, W., and Tomic, J. (2005). Vehicle-to-grid power fundamentals: calculating capacity and net revenue. *J. Power Sources* 144, 268–279. doi:10.1016/j.jpowsour.2004.12.025

Keshan, H., and Thornburg, J. (2016). "Comparison of lead-acid and lithium ion batteries for stationary storage in off-grid energy systems," in *4th IET clean energy and technology conference (CEAT 2016)*. Malaysia: Kuala Lumpur, 1–7.

Lalhmachhuana, R., Deb, S., Datta, S., Singh, K. R., Cali, U., and Ustun, T. S. (2024). Multi-objective-based economic and emission dispatch with integration of wind energy sources using different optimization algorithms. *Front. Energy Res.* 12, 1421212. doi:10.3389/fenrg.2024.1421212

Latif, A., Hussain, S. M. S., Das, D. C., and Ustun, T. S. (2021). Double stage controller optimization for load frequency stabilization in hybrid wind-ocean wave energy based maritime microgrid system. *Appl. Energy* 282, 116171. doi:10.1016/j.apenergy.2020.116171

Latif, A., Paul, M., Das, D. C., Hussain, S. M. S., and Ustun, T. S. (2020). Price based demand response for optimal frequency stabilization in ORC solar thermal based isolated hybrid microgrid under salp swarm technique. *Electronics* 9 (12), 2209. doi:10.3390/electronics9122209

Ma, H. P., Yang, Z. L., You, P. C., and Fei, M. R. (2017). Multi-objective biogeography-based optimization for dynamic economic emission load dispatch considering plug-in electric vehicles charging. *Energy* 135, 101–111. doi:10.1016/j.energy.2017.06.102

Madawala, A. K., and Thrimawithana, D. J. (2011). A bidirectional inductive power interface for electric vehicles in V2G systems. *IEEE Trans. Ind. Electron.* 58 (10), 4789–4796. doi:10.1109/tie.2011.2114312

Nourianfar, H., and Abdi, H. (2023). Economic emission dispatch considering electric vehicles and wind power using enhanced multi-objective exchange market algorithm. *J. Clean. Prod.* 415 (2023), 137805, June. doi:10.1016/j.jclepro.2023.137805

Nsonga, P., Hussain, S. M. S., Garba, A., and Ali, I. (2017). "Performance evaluation of electric vehicle ad-hoc network technologies for charging management," in *2017 IEEE PES asia-pacific power and energy engineering conference*. Bangalore, India: APPEEC, 1–5.

Peng, M., Liu, L., and Jiang, C. (2012). A review on the economic dispatch and risk management of the large-scale plug-in electric vehicles (PHEVs)-penetrated power systems. *Renew. Sustain. Energy Rev.* 16 (3), 1508–1515. doi:10.1016/j.rser.2011.12.009

Ranjan, S., Jaiswal, S., Latif, A., Das, D. C., Sinha, N., Hussain, S. M. S., et al. (2021). Isolated and interconnected multi-area hybrid power systems: a review on control strategies. *Energies* 14, 8276. doi:10.3390/en14248276

Saber, A. Y., and Venayagamoorthy, G. K. (2011). Plug-in vehicles and renewable energy sources for cost and emission reductions. *IEEE Trans. Ind. Electron.* 58 (4), 1229–1238. doi:10.1109/tie.2010.2047828

Safiullah, S., Rahman, A., Lone, S. A., Hussain, S. S., and Ustun, T. S. (2022). Robust frequency–voltage stabilization scheme for multi-area power systems incorporated with EVs and renewable generations using AI based modified disturbance rejection controller. *Energy Rep.* 8, 12186–12202. doi:10.1016/j.egyr.2022.08.272

Sahoo, A., Hota, P. K., Sahu, P. R., Alsaif, F., Alsulamy, S., and Ustun, T. S. (2023). Optimal congestion management with FACTS devices for optimal power dispatch in the deregulated electricity market. *Axioms* 12, 614. doi:10.3390/axioms12070614

Sahoo, A., Sahu, P. R., Hota, P. K., Islam, M. M., and Ustun, T. S. (2024). Optimal dispatch of combined heat and power generating units with prohibited operating zones

using improved heap-based optimizer. *IET Gener. Transm. Distrib.* 18, 79–96. doi:10.1049/gtd2.13070

Sen, T., and Mathur, H. D. (2016). A new approach to solve Economic Dispatch problem using a Hybrid ACO-ABC-HS optimization algorithm. *Int. J. Elect. Power Energy Syst.* 78, 735–744. doi:10.1016/j.ijepes.2015.11.121

Shargh, S., Khorshid ghazani, B., Mohammadi-ivatloo, B., Seyedi, H., and Abapour, M. (2016). Probabilistic multi-objective optimal power flow considering correlated wind power and load uncertainties. *Renew. Energy* 94, 10–21. doi:10.1016/j.renene.2016.02.064

Shazly, A. M., Anwer, N., and Metwally Mahmoud, M. (2023). Solving optimal power flow problem for IEEE-30 bus system using a developed particle swarm optimization method: towards fuel cost minimization. *Int. J. Model. Simul.*, 1–14. doi:10.1080/02286203.2023.2201043

Singh, S. P., Tyagi, R., and Goel, A. (2014). Genetic algorithm for solving the economic load dispatch. *Int. J. Electron. Electr. Eng.* 7, 523–528.

Sioshansi, R., and Denholm, P. (2009). Emissions impacts and benefits of plug-in hybrid electric vehicles and vehicle-to-grid services. *Environ. Sci. Technol.* 43, 1199–1204. doi:10.1021/es802324j

Srivastava, A. K., Annabathina, B., and Kamalasadan, S. (2010). The challenges and policy options for integrating plug-in hybrid electric vehicle into the electric grid. *Elect. J.* 23, 83–91. doi:10.1016/j.tej.2010.03.004

Tappeta, V. S. R., Appasani, B., Patnaik, S., and Ustun, T. S. (2022). A review on emerging communication and computational technologies for increased use of plug-in electric vehicles. *Energies* 15 (18), 6580. doi:10.3390/en15186580

Tawfak Al-Bahrani, L., Ben, H., Mehdi, S., and Alex, S. (2020). Dynamic economic emission dispatch with load dema nd management for the load demand of electric vehicles during crest shaving and valley filling in smart cities environment. *Energy* 195, 116946. doi:10.1016/j.energy.2020.116946

Ustun, T. S., Hussain, M., Syed, M. H., and Dambrauskas, P. (2021). IEC-61850-Based communication for integrated EV management in power systems with renewable penetration. *Energies* 14, 2493. doi:10.3390/en14092493

Ustun, T. S., Zayegh, A., and Ozansoy, C. (2013). Electric vehicle potential in Australia: its impact on smartgrids. *IEEE Ind. Electron. Mag.* 7 (4), 15–25. doi:10.1109/mie.2013.2273947

Wei, Y., Yao, Y., Pang, K., Xu, C., Han, X., Lu, L., et al. (2022). A comprehensive study of degradation characteristics and mechanisms of commercial Li(NiMnCo)O$_2$ EV batteries under vehicle-to-grid (V2G) services. *J. Battery Energy Storage Adv. power Syst.* 8 (10), 188. doi:10.3390/batteries8100188

Wood, A. J., Wollenberg, B. F., and Sheble, G. B. (2012). *Power generation, operation, and control.* 3rd edn. New York, NY, USA: Wiley.

Xie, T., Su, Y., Zhang, G., Zhang, K., Li, H., and Wang, R. (2024). Optimizing peak-shaving cooperation among electric vehicle charging stations: a two-tier optimal dispatch strategy considering load demand response potential. *Electr. Power Energy Syst.* 162 (2024), 110228. doi:10.1016/j.ijepes.2024.110228

Xing, H., Fu, M., Lin, Z., and Mou, Y. (2016). Decentralized optimal scheduling for charging and discharging of plug-in electric vehicles in smart grids. *IEEE Trans. Power Syst.* 31 (5), 4118–4127. doi:10.1109/tpwrs.2015.2507179

Yao, W., Zhao, J., Wen, F., Xue, Y., and Ledwich, G. (2013). A hierarchical decomposition approach for coordinated dispatch of plug-in electric vehicles. *IEEE Trans. Power Syst.* 28 (3), 2768–2778. doi:10.1109/tpwrs.2013.2256937

Zou, D., Li, S., Xuan, K., and Ouyang, H. (2022). A NSGA-II variant for the dynamic economic emission dispatch considering plug-in electric vehicles. *Comput. and Industrial Eng.* 173, 108717. doi:10.1016/j.cie.2022.108717

Glossary

ED	Economic dispatch
PSO	Particle swarm optimization
EVs	Electric vehicles
PEVs	Plug-in electric vehicles
PHEVs	Plug-in hybrid electric vehicles
NiMH	Nickel-metal hydride
Li-ion	Lithium ion
$Li(NiMnCo)O_2$	Lithium nickel manganese cobalt oxide
V2G	Vehicle-to-grid
G2V	Grid-to-vehicle
ALO	Ant-lion optimization
$|V|^{(initial)}$	Initial voltage magnitude
$\delta^{(initial)}$	Initial voltage angle
$\Delta P_{calc}^{(initial)}$	Real power injected
$\Delta P^{(initial)}$	Change in real power
$\Delta Q_{calc}^{(initial)}$	$\Delta Q^{(initial)}$ Reactive power injected
$\Delta Q^{(initial)}$	Change in reactive power
$I^{(initial)}$	Initial Jacobian matrix
X_p	pth grasshopper position
S_p	pth grasshopper social interaction
G_p	Gravitational force
A_p	Wind advection
s	Social force between the grasshopper
f	Generation cost comparison during discharging using MOALO
y	Distance between the grasshopper
kk	Length of attraction
x_p^z	zth variable pth position in the population
D_{pq}^z	Distance between the pth and qth position of the zth variable
x_{gbest}^z	Global best of zth variable
G	Parameter of the GOA
N	Number of thermal units
a_i, b_i, and c_i	Cost coefficients of the ith unit
P_i	Active power output of the ith generator
V_i and θ_i	Voltage magnitude and voltage angle at bus i
$G_{q(ij)}$	Transfer conductance between bus i and bus j
NL	Number of transmission lines
P_{V2G} and P_{G2V}	Discharging power and charging load of EVs, respectively
P_D and P_L	Power load demand and power loss of the system, respectively
P_{G_q} and P_{D_q}	Real power generation and real power demand at yth bus, respectively
V_y and V_a	Voltage magnitude at yth and ath bus, respectively
G_{ya} and B_{ya}	Conductance and susceptance of yth and ath bus, respectively
V_{Gp} and P_{Gp}	Voltage magnitude and real power generation, respectively

N_G	Number of generating units
V_{Lr}	Voltage magnitude of load bus r
S_{ln}	Power at branch N_{BR}
Obj_i^{min} and Obj_i^{max}	Least and greatest value of the objective function, respectively
N_{obj}	Number of objectives
N	Number of non-dominated solutions
M_d	Daily driven miles of an EV
μ_m and σ_m	Mean and standard variation of M_d M_d
E_m and β	Energy consumption and battery capacity of each EV
M_{dmax}	Maximum achievable driven distance
E_d	Expected energy demand of EV
t_{ar}, t_{dep}, and t_d	Arrival time, departure time, and expected duration of parking, respectively
N_1 and N_2	Normally distributed random variables
μ_{ar} μ_m and μ_{dep} μ_m	Mean value of the arrival time and the departure time
σ_{ar} and σ_{dep}	Standard deviation of the arrival time and the departure time
SOC_d	Desired state of charge
Chr	Charging rate
SOC_{ini}	Initial state of charge
SOC_f	Final state of charge